

Ph. D Dissertation

**Magnetic Anisotropy Control Methods in Soft Magnetic
Thin Film and Magnetic Sensor Applications**

軟磁性薄膜の磁気異方性制御とセンサ応用

Shin, Jaewon

Department of Electrical Engineering
Graduate School of Engineering,
TOHOKU UNIVERSITY

Committee in charge

Professor, Kazushi Ishiyama, Chair

Professor, Masashi Sahashi

Professor, Hiroaki Muraoka

Associate Professor, Shuichiro Hashi

2015

Abstract

The giant magnetoimpedance (GMI) effect has been widely investigated due to its potential application in sensor elements. The GMI effect is studied in wires, ribbons or single layered thin films, and multi-layered thin films. Multi-layered thin films show a noticeable increase in the GMI effect. The GMI sensor element shows high MI effect with transverse magnetic anisotropy. However, it is difficult to induce magnetic anisotropy in transverse direction of the element due to a large demagnetizing field. Therefore, the focus of this thesis work is to explore simple and effective methods to control the direction of the magnetic anisotropy and to fabricate magnetic anisotropy which rapidly reacts to a weak external magnetic field for sensor applications. I proposed an original method to induce and control magnetic anisotropy using the inverse-magnetostrictive effect (also known as the Villari effect) and residual stress, which is generated by different thermal expansion coefficients between layers in the multi-layered structure. The proposed method was verified by Finite Elements Method (FEM) simulations and experiments. I also investigated the variation of magnetic properties with changes in the geometry of the elements as well as magnetic materials for inducing magnetic anisotropy whose direction can be changed by a weak external magnetic field. Based on the proposed method, the prototype sensor elements were manufactured. The performance of the prototype sensor elements was examined. It showed impedance variation by applying a weak external magnetic field. The results confirm that the proposed method to induce magnetic anisotropy is effective. Furthermore, the fabricated sensor elements work as a magnetic sensor.

TABLE OF CONTENTS

ABSTRACT	i
TABLE OF CONTENTS.....	iii
LIST OF FIGURES	vi
LIST OF TABLES	xi
Chapter 1 Introduction	1
1.1 Introduction.....	1
1.2 Purpose of Anisotropy Control Study.....	2
1.2.1 Inducing Transverse Magnetic Anisotropy.....	3
1.2.2 Strength Control of Magnetic Anisotropy	3
1.3 Construction of the Thesis	4
References	5
Chapter 2 Literature review	9
2.1 Introduction.....	9
2.2 Classification of Magnetic Sensors	10
2.3 Theory of Giant Magneto-Impedance Effect.....	18
2.3.1 GMI in wires	18
2.3.2 GMI in ribbons or single layered thin films.....	19
2.3.3 GMI in multi-layered thin films	20
References	23
Chapter 3 Inducing and Controlling Mechanism of Magnetic Anisotropy	27
3.1 Introduction.....	27
3.2 Methodology of Direction Control of In-plane Uniaxial Magnetic Anisotropy	30

3.3 Verification by FEM Simulation.....	38
3.4 Fabrication of Thin film.....	40
3.5 Experimental Result.....	46
3.6 Summary.....	49
References.....	50

Chapter 4 Investigation of Magnetic Properties According to Changes in

Geometry of Elements.....	53
4.1 Introduction.....	53
4.2 Influence of Ratio of the Thickness on Magnetic Anisotropy.....	55
4.2.1 Calculations of generated stress and shape anisotropy.....	55
4.2.2 Experimental analysis.....	61
4.3 Influence of Width of Magnetic Layer on Magnetic Anisotropy.....	66
4.3.1 Fabrication of the elements.....	66
4.3.2 Experimental results according to changes in width of the magnetic layer.....	66
4.4 Influence of Length of Conductive Layer on Magnetic Anisotropy.....	75
4.4.1 Fabrication of the elements.....	75
4.4.2 Experimental results according to changes in length of the conductive layer.....	75
4.4.3 Experimental results according to changes in shape of the conductive layer.....	80
4.5 Summary.....	82
References.....	83

Chapter 5 Investigation of Magnetic Properties According to Changes in

Magnetic Material.....	85
5.1 Introduction.....	85
5.2 Variation of Composition in CoFeSiB.....	87

5.3 Magnetic Properties of CoFeSiB Samples by Changes in Magnetostriction Constant	92
5.4 Summary	98
References	99
Chapter 6 Sensor Application	101
6.1 Introduction	101
6.2 Experimental Analysis	102
6.2.1 Impedance measurement according to changes in length of conductive layer.....	102
6.2.2 Impedance measurement according to changes in magnetostriction constant	109
6.3 Comparison with Current Magnetic Sensor	111
6.4 Summary	114
References	115
Chapter 7 Conclusion	119
7.1 Conclusion and Discussion.....	119
7.2 Suggestions for Future Works	120
List of Achievements	123
Acknowledgement	127

LIST OF FIGURES

Chapter 2 Literature review

Figure 2.1 Applications of search-coil

Figure 2.2 The basic fluxgate principle. I_{exc} is ac current of drive coil. The core permeability is $\mu(t)$. B_0 is measured dc field and V_{ind} is induced in the sense coil

Figure 2.3 Fluxgate operating principle

Figure 2.4 Schematic of SQUID

Figure 2.5 Schematic of Hall effect sensors

Figure 2.6 Application of MI sensors (a) Electrical compass (b) Motion control sensor for cell phone

Figure 2.7 A summary of the various magnetic sensors sensitivity

Figure 2.8 Wire type MI sensor element with domain structure

Figure 2.9 Ribbon type MI sensor element with domain structure

Figure 2.10 Multi-layered type MI sensor element with domain structure

Figure 2.11 A relationship between direction of magnetic anisotropy and permeability in multi-layered thin film structure

Chapter 3 Inducing and Controlling Mechanism of Magnetic Anisotropy

Figure 3.1 The configuration of the change of the permeability according to apply the external magnetic field and carrier current

Figure 3.2 Principle of Inverse-Magnetostriction

Figure 3.3 Bending direction in the multilayer structure according to changes in the combination of thermal expansion coefficients between layers

Figure 3.4 A configuration of deposited thin-film: The fabricated thin-films consist of magnetic layer and conductive layer

Figure 3.5 A relationship between inner force and residual stress in the rectangular shape: denotes the inner compressive (shrink) force

Figure 3.6 Direction of residual stress in the magnetic layer according to direction of inner forces

Figure 3.7 FEM simulation of residual stress distribution using quarter model

Figure 3.8 A structure and size of the thin film

Figure 3.9 A process of the thin film fabrication

Figure 3.10 Annealing condition

Figure 3.11 A result of the magnetic domain observation in the magnetic layer with Mo conductive layer

Figure 3.12 A result of the magnetic domain observation in the magnetic layer with Ti conductive layer

Chapter 4 Investigation of Magnetic Properties According to Changes in Geometry of Elements

Figure 4.1 (a) Thin film structure. (b) Positive bending caused by the different thermal expansion coefficients under cooling

Figure 4.2 Neutral plane between the two deposited layers. The dotted line denotes the neutral plane

Figure 4.3 Calculation results: radius of curvature and bending stress

Figure 4.4 Calculated shape magnetic anisotropy for various thicknesses of the magnetic layer

Figure 4.5 Schematic of the fabricated thin films and their observed domains for various thicknesses of the magnetic layer

Figure 4.6 VSM measurement results for the H_k Total between the width and the length direction

Figure 4.7 $H_{k(t)}$ result obtained from VSM measurements

Figure 4.8 Analysis of the magnetic anisotropy: $H_{k(t)}$, $H_{k(s)}$, and $H_{k(i)}$

Figure 4.9 Relationship between bending stress and induced magnetic anisotropy

Figure 4.10 (a) Schematic of the sensor structure. The red box denotes the point of the domain observation. The width of the sensor changed from 40 μm to 800 μm . The thickness of the magnetic layer was varied at 0 μm , 1.4 μm , and 2.1 μm . (b) Fabricated sensors (100 μm –500 μm)

Figure 4.11 Results of the magnetic domain observation with narrow width sensor at (a) 40 μm and (b) 50 μm

Figure 4.12 Calculation of the demagnetizing field versus the changes in width

Figure 4.13 Magnetization curves according to changes in the width: (a) Result of the transverse measurement, and (b) result of the longitudinal measurement

Figure 4.14 Results of magnetic domain observation using Kerr-effect microscopy. The width of magnetic anisotropy increased with the sample width

Figure 4.15 A configuration of fabricated thin film according to changes in length of Molybdenum conductive layer. Gray and orange color denotes the magnetic and conductive layer, respectively

Figure 4.16 A process to change stress difference according to changes in length of conductive layer

Figure 4.17 A configuration of fabricated thin film according to changes in length of Molybdenum conductive layer. Gray and orange color denotes the magnetic and conductive layer, respectively

Figure 4.18 A result of H_k measurement according to changes in length of Molybdenum conductive layer

Figure 4.18 A configuration and the results of magnetic domain observation. (a) The shape

of magnetic and conductive layer is isomorphic. (b) The conductive layer has rectangular shape under the entire area of patterned magnetic layer

Chapter 5 Investigation of Magnetic Properties According to Changes in Magnetic Material

Figure 5.1 Configuration of fabricated element. (a) Top view (b) Cross section view from a to a'

Figure 5.2 A method of CoFeSiB composition. Using $\text{Co}_{70}\text{Si}_{17}\text{B}_{13}$ with pure Fe chips, the magnetostriction constant is controlled

Figure 5.3 Results of magnetic domain observation of the central area of the magnetic layer. (a) FeSiB magnetic layer. (b) CoFeSiB magnetic layer

Figure 5.4 Domain patterns observed during magnetization along the longitudinal direction using Kerr-effect microscopy. (a) FeSiB layer (b) CoFeSiB layer

Figure 5.5 Magnetization curves according to changes in magnetostriction constant. Hysteresis loops with external magnetic field applied along the (a) longitudinal and (b) transverse directions of the element

Figure 5.6 Magnetic domain observation for detection of transverse magnetic anisotropy. (a) Magnetostriction constant is nearly zero (0×10^{-6}) (b) Magnetostriction constant is negative (-4×10^{-6})

Chapter 6 Sensor Application

Figure 6.1 Configuration of impedance measurement system: ① Helmholtz coil, ② Microscope, ③ Soucemeter, ④ Network analyzer, ⑤ Sample stage. (b) Probe for measurement and picture of the mounted element

Figure 6.2 (a) Configuration of fabricated thin film according to changes in the length of conductive layer (b) Measured anisotropy field (H_k)

Figure 6.3 Configuration of the fabricated MI sensor elements (a) Length of conductive layer is 4.6 mm (b) 4.2 mm (c) 3.4 mm (d) 1.8 mm

Figure 6.4 Hysteresis loops measuring transverse and longitudinal direction according to

changes in length of the conductive layer

Figure 6.5 The results of impedance measurement with changes in the length of conductive layer from 4.6 mm to 1.8 mm

Figure 6.6 (a) A Configuration of fabricated element and Results of impedance measurement at 100 MHz. The external magnetic field was applied from -16 Oe to +16 Oe.
(a) FeSiB layer (b) CoFeSiB layer

Figure 6.7 Evaluated resolution of fabricated sensor element. Star maker denotes the prospected resolution

Figure 6.8 Comparison of performance cost of the magnetic sensors

LIST OF TABLES

Chapter 3 Inducing and Controlling Mechanism of Magnetic Anisotropy

Table 3.1 The mechanical properties of the target materials

Table 3.2 Sputtering condition of each material

Chapter 4 Investigation of Magnetic Properties According to Changes in Geometry of Elements

Table 4.1 Divided into shape anisotropy and induced anisotropy

Chapter 5 Investigation of Magnetic Properties According to Changes in Magnetic Material

Table 5.1 Sputtering condition

Table 5.2 Composition rate and its magnetostriction constant

Chapter 6 Sensor Applications

Table 6.1 Comparison of thin film type MI sensor elements

Chapter 1

Introduction

1.1 Introduction

The giant magnetoimpedance (GMI) effect has been studied extensively due to its potential application in sensor elements [1]–[6]. The GMI effect is basically caused by the change in impedance of magnetic material when an external magnetic field is applied. This effect in soft magnetic material is developed in wires [7]–[10], ribbons or single layered thin films [11]–[13], and multi-layered thin films [14]–[18]. Among the different geometries of GMI elements, the multi-layered geometry shows the most substantial MI effect. Thus, the higher sensitivities have been reported in multi-layered MI elements.

In spite of advances in GMI effect, it is not enough to utilize commercial magnetic sensor elements even though it has very attractive potential and performance (large change of impedance).

The focus of this thesis work is to explore direction control of the magnetic

anisotropy using a simple and effective method and to fabricate magnetic anisotropy which rapidly reacts to a weak external magnetic field for application to sensors. I propose an original method to induce and control magnetic anisotropy using the inverse-magnetostrictive effect (also known as the Villari effect) and residual stress, which is generated by different thermal expansion coefficients between layers in the multi-layered structure. The proposed method was verified by simulations and experiments. I also investigated the variation of magnetic properties with changes in the geometry of the elements and magnetic materials. I found that I could induce and control the direction of magnetic anisotropy. Moreover, the strength of the induced magnetic anisotropy could be controlled by changing the geometrical properties (the aspect ratio between length and width or the thickness ratio between the magnetic and conductive layers).

Based on the proposed method, the prototype sensor elements were manufactured. The performance of the prototype sensor elements was examined. It showed impedance variation in response to a weak external magnetic field. From the results, I could confirm that the proposed method to induce magnetic anisotropy is effective. Furthermore, the fabricated sensor elements work as a magnetic sensor.

1.2 Purpose of Anisotropy Control Study

In this study, I propose a new magnetic anisotropy control method using the inverse-magnetostrictive effect and residual stress which produced by different of thermal expansion coefficients in the bimetal structure. The new anisotropy control method can simply induce transverse magnetic anisotropy in the rectangular shaped bimetal

structure thin films to improve the sensitivity of an MI sensor. Furthermore, I examine the relationship between magnetic anisotropy and the geometrical properties of the elements for the precision anisotropy control.

1.2.1 Inducing Transverse Magnetic Anisotropy

A significant change in permeability is required to improve the sensitivity of the MI sensor. The change can be realized by inducing transverse magnetic anisotropy. In general, transverse magnetic anisotropy can be induced by several methods: deposition in magnetic field, annealing within a rotating and static magnetic field, and stress bias annealing. However, these methods have inconveniences. For instance, in the case of the stress bias annealing, additional equipment is necessary to bend the substrate and thin film. In addition, there is a risk of cracking or breaking the substrate. Therefore, a simpler and safer method is required.

I propose a method to induce transverse magnetic anisotropy inducing method in rectangular bimetal thin films. I produced stresses in the thin film using the difference in thermal expansion coefficients between layers without additional equipment or bending of substrates. The generated stress can induce the magnetic anisotropy of magnetostrictive material magnetic film.

1.2.2 Strength Control of Magnetic Anisotropy

A transverse magnetic anisotropy can improve the sensitivity of the MI sensors. Furthermore, control of magnetic anisotropy strength is necessary to precisely manipulate the sensitivity of the MI sensors. The strength of the magnetic anisotropy can be controlled according to changes in geometrical properties, such as each layer's

length and thickness. Besides, in this study, I can confirm the fabrication region because I use the residual stresses and the stresses are determined by the combination of the thickness and length in two layers. Therefore, according to changes in the geometrical properties, I confirm the strength of the magnetic anisotropy by Kerr-microscope and VSM.

1.3 Construction of the Thesis

The construction of the thesis is structured as follows.

Chapter 1 is an introduction. I introduce the motivation and purpose of this study.

In chapter 2, current magnetic sensor technologies and the general magneto-impedance effect are discussed.

Chapter 3 deals with inducing and controlling mechanism of magnetic anisotropy. I propose a new method to induce magnetic anisotropy and confirm the proposed method by FEM simulations and experiments.

Chapter 4 deals with controlling the magnetic anisotropy field strength control by changing the geometry of the elements. I evaluate how the magnetic anisotropy field strength varies in response to changes in the thickness and length of the layers through magnetic domain observation and VSM measurement.

Chapter 5 discusses how the magnetic anisotropy field strength is controlled by changes in magnetic material. In this chapter, I examine the relationship between the strength of induced magnetic anisotropy and the magnetostriction constant.

Chapter 6 describes how the method can be applied to sensors. I carry out impedance measurements using a fabricated prototype sensor element with the proposed method.

Chapter 7 is conclusion. In this chapter, I summarize the magnetic anisotropy control method and the experimental results.

References

- [1] L. Panina and K. Mohri, “Magneto-impedance effect in amorphous wires,” *Appl. Phys. Lett.*, **65**, 1189-1191, 1994.
- [2] L. Kraus, “Theory of giant magneto-impedance in the planar conductor with uniaxial magnetic anisotropy,” *J. Magn. Magn. Mater.*, **195**, 764-778, 1999.
- [3] T. Uchiyama, K. Mohri, Y. Honkura, and L. V. Panina, “Recent Advances of Pico-Tesla Resolution Magneto-Impedance Sensor Based on Amorphous Wire CMOS IC MI Sensor,” *IEEE Trans. Magn.*, **48**, 3833-3839, 2012.
- [4] T. Morikawa, Y. Nishibe, H. Yamadera, Y. Nonomura, M. Takeuchi, and Y. Taga, “Giant Magneto-Impedance Effect in Layered Thin Films,” *IEEE Trans. Magn.*, **33**, 4367-4372, 1997.
- [5] Y. Murayama, T. Ozawa, S. Yabukami, K. Ishiyama, and K.I. Arai, “High-Frequency Carrier-Type Magnetic Field Sensor with a Sub-pT Resolution Using a Magnetic Film and a Transmission Line,” *J. Magn. Soc. Jpn*, **31**, 17-22, 2007.
- [6] L. V. Panina, K. Mohri, K. Bushida, and M. Noda, “Giant magnetoimpedance and magnetoinductive effects in amorphous alloys”, *J. Appl. Phys.*, **76**, 6198, 1994.
- [7] M. Tejedor, B. Hernando, M. L. Sanchez, V. M. Prida, J. M. Garcia-Beneytez M. Vazquez, and G. Herzer, “Magneoimpedance effect in zero magnetostriction nanocrystalline Fe_{73.5}Cu₁Nb₃Si_{16.5}B₆ ribbons”, *J. Mag. Mag. Mat.*, **185**, 61-65, 1998.
- [8] D. Garcia, G. V. Kurlyanskaya, M. Vazquez, F. I. Toth, and L. K. Varga, “Influence of field annealing on the hysteretic behavior of the giant magneto-

- impedance effect of Cu wires covered with Ni₈₀Fe₂₀ outer shells,” *J. Mag. Mag. Mat.*, **203**, 208-210, 1999.
- [9] K. R. Pirota, L. Kraus, H. Chiriac, and M. Knobel, “Magnetic properties and giant magnetoimpedance in a CoFeSiB glass-covered microwire,” *J. Mag. Mag. Mat.*, **221**, 243-247, 2000.
- [10] M. Vazquez, “Giant magneto-impedance in soft magnetic “wires”,” *J. Mag. Mag. Mat.*, **226-260**, 693-699, 2001.
- [11] C. G. Kim, K. J. Jang, H. C. Kim and S. S. Yoon, “Asymmetric giant magnetoimpedance in field-annealed Co-based amorphous ribbon,” *J. Appl. Phys.*, **85**, 5447, 1999.
- [12] H. Q. Guo, H. Kronmuller, T. Dragon, Z. H. Gheng, and B. G. Shen, “Influence of nanocrystallization on the evolution of domain patterns and the magnetoimpedance effect in amorphous Fe_{73.5}Cu₁Nb₃Si_{13.5}B₉ ribbons,” *J. Appl. Phys.*, **89**, 514, 2001.
- [13] G. V. Kurlyandskaya, J.M. Barandiaran, M. Vazquez, D. Garcia, and N.V. Dmitrieva, “Influence of geometrical parameters on the giant magnetoimpedance response in amorphous ribbon,” *J. Mag. Mag. Mat.*, **215-216**, 740-742, 2000.
- [14] K. Hika, L. V. Panina, and K. Mohri, “Magneto-Impedance in Sandwich Film for Magnetic Sensor Heads”, *IEEE Trans. Magn.*, **32**, 4594-4596, 1996.
- [15] D. de Cos, L. V. Panina, N. Fry, I. Orue, A. Garcia-Arribas, and J. M. Barandiaran, “Magnetoimpedance in Narrow NiFe/Au/NiFe Multilayer Film Systems,” *IEEE Trans. Magn.*, **41**, 3697-3699, 2005.
- [16] A. V. Svalov, E. Fernandez, A. Garcia-Arribas, J. Alonso, M. L. Fdez-Gubieda, and G. V. Kurlyandskaya, “FeNi-Based magnetoimpedance multilayers: Tailoring

of the softness by magnetic spacers,” *Appl. Phys. Lett.*, **100**, 162410, 2012.

- [17] P. Delooze, L. V. Panina, and D. J. Mapps, “AC Biased Sub-Nano-Tesla Magnetic Field Sensor for Low-Frequency Applications Utilizing Magnetoimpedance in Multilayer Films.” *IEEE Trans. Magn.*, **41**, 3652-3654, 2005.
- [18] S. O. Volchkov, E. Fernández, A. García-Arribas, J. M. Barandiaran, V. N. Lepalovskij, and G. V. Kurljanskaya, “Magnetic Properties and Giant Magnetoimpedance of FeNi-Based Nanostructured Multilayers With Variable Thickness of the Central Cu Lead,” *IEEE Trans. Magn.*, **47**, 3328-3331, 2011.

Chapter 2

Literature Review

2.1 Introduction

A sensor is devices that respond various physical quantities and converts these into signals. The term a sensor has widely used in the present. Recently, an importance of sensors increases with development of electric and electronic engineering, because sensors have used almost all of the industrial settings or equipments.

The magnetic sensors have assisted humankind for many years for measuring and controlling a lot of functions [1]. Since the discovering of magnetic compass, the magnetic sensors have made remarkable progress. Present magnetic sensors have expanded the scope of use such as position control of the satellite by flux-gate magnetic sensor [2, 3] and reading the magnetoencephalography [4] and magnetocardiogram [5].

Many of magnetic and electric phenomena which have used in magnetic sensor applications were discovered toward the 19th and 20th centuries. Therefore, recent researches of the magnetic sensor focused on the development of new materials or new

sensor design more than new principles. Furthermore, because of mobility and energy problems, magnetic sensors require low power consumption and miniaturization.

The classification of magnetic sensors and basic research of magnetic phenomena is requirement as a preliminary research.

2.2 Classification of Magnetic Sensors

Magnetic sensors can be classified according to principle of operations. In this chapter, I classified magnetic sensor and discussed a couple of important principles for magnetic sensor application.

A number of magnetic phenomena have used for magnetic sensor applications.

- Faraday's law of induction
- Change of inductance and eddy-current effect
- Alteration of induced electromotive force by changes in magnetic flux density
- Joule effect
- ΔE effect
- Matteucci effect
- Hall effect
- Thomson effect
- Vallari effect
- Curie temperature and Hopkinson effect

There are many ways to detect magnetic field, such as above. Almost all the methods based on the intimate relation between electric and magnetic phenomena.

(a) Search-Coil Sensor

The Faraday's law of induction is used for the principle of search-coil sensor. A typical search-coil sensor consists of a multilayer solenoid coil. When the magnetic flux through the multilayer solenoid coil, a current is induced and a voltage is generated between its leads proportionally to the change of the flux.

In general, the ferromagnetic core with a high magnetic permeability is inserted inside of coil. It has larger sensitivity, but it is less stable than without core. It should be long and thin due to a low demagnetization. Furthermore, recent search coil are usually operating in the current-output mode.

This type sensor can detect fields as weak as 2×10^{-5} nT, and there is no upper limitation. These sensors are used in various applications as shown Figure 2.1. The search coil sensor is mainly used in rough environment such as aircraft door or landing gear [1].

(b) Fluxgate Sensor

Fluxgate sensors sense the magnitude and direction of the dc or low-frequency ac magnetic field. The basic sensor principle is illustrated in Fig. 2.2. The fluxgate sensor consists of a soft magnetic material core and two coils, drive and sense coil. The magnetic core is periodically saturated by sufficiently large sinusoidal current which is applied to the drive coil, hence the core permeability changes, and the dc flux is modulated. The operation conditions are determined on either saturation or non saturation regions, as shown in Figure 2.3. In the saturation, the reluctance of the core increases. Therefore, it makes that the any additional magnetic field to pass the core is less attractive. When the current in the drive coil reduces, the core comes out of

saturation. The external magnetic field is attracted to the core. This change detects by the sense coil and the output signal is proportional to the external magnetic field.

The sensitivity of fluxgate sensor depends on the shape of the hysteresis loop. To obtain high-sensitivity, B-H loop should be square due to it produces the highest induced electromotive force. In addition, for the low power consumption, the low coercivity and saturation value require. Generally, the sensitivity range of fluxgate sensor is from 10^{-2} to 10^7 nT. The fluxgate sensor is similar search-coil in size, but fluxgate sensor needs five times as much power. Compare with search-coil, it has advantage for ability of precision dc fields measurement. This type sensors have used for not only observing changes in the Earth's magnetic field but also aircraft and vehicle navigation.

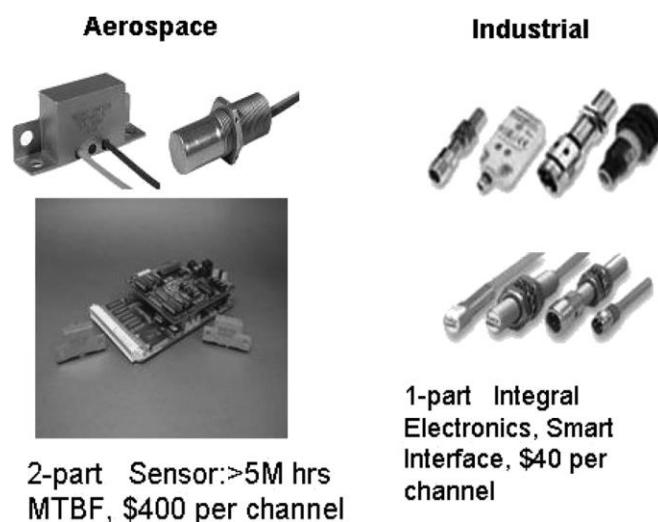


Figure 2.1 Applications of search-coil

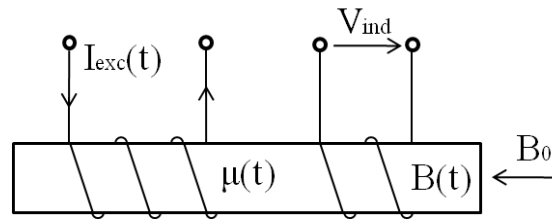


Figure 2.2 The basic fluxgate principle. I_{exc} is ac current of drive coil. The core permeability is $\mu(t)$. B_0 is measured dc field and V_{ind} is induced in the sense coil

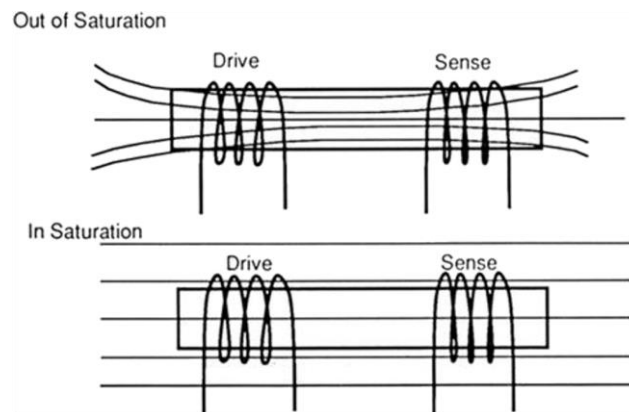


Figure 2.3 Fluxgate operating principle

(c) SQUID Sensor

Superconducting Quantum Interference Devices (SQUIDs) sensors are the most sensitive of all devices for measuring a magnetic field at low frequency. At temperature approaching absolute zero, certain materials become superconductors and the resistance of materials dropped to an immeasurably small value.

Typically, ring type superconducting is used for detection of magnetic field. In the normal (above transition temperature) state, magnetic flux lines can penetrate through a ring. When the temperature cools down below transition temperature, the material becomes superconducting and the magnetic flux is expelled and the interior flux is trapped. If the magnetic field is extinguished, the current is induced and it would continue flowing eternally. The magnitude of current elaborately represents the magnetic flux density. To measure the current, we can detect the magnetic field as shown in Fig. 2.4.

The sensitivity of SQUIDs sensor is determined by the magnetic field noise. In general, the noise of commercial DC SQUIDs is 10^{-5} nT. Therefore, SQUID sensors are used in bio-signal sensing applications.

(d) Hall Effect Sensor

A Hall effect magnetic sensors are the most widely used magnetic sensors due to their simplicity, good characteristics and compatibility. The physical phenomenon which is used for this type sensor is discovered by Edwin H. Hall more than 100 years ago.

Usually, semiconductors are used because the Hall effect is much larger in semiconductors than metallic conductors. When a current is applied along the length of thin semiconductor placed in a magnetic field perpendicular to the plane of the rectangle, a voltage difference generates across the thin semiconductor as shown in Figure 2.5. A

moving electron veers off in one direction by magnetic field.

The sensitivity of silicon type Hall magnetic sensor is around 10^6 to 10^8 nT. The Hall magnetic sensor is rarely used to sense just a magnetic field. It is used for a component of contactless position, velocity, and rotation sensor.

(e) Magnetoimpedance (MI) Sensor

When the high frequency current is applied to the soft magnetic materials, permeability of the materials is changed by an external magnetic field. According to the changes in permeability, the skin depth is determined. This skin depth causes change of impedance. Therefore, we can detect the magnetic field from the impedance changes. MI sensors have similar or much higher sensitivity without use of exciting and sensing coil compare to fluxgate sensors. Furthermore, high sensitive MI sensor has been reported in the room temperature [6]. It has about 10^{-13} T resolution. In other word, the resolution of MI sensors is equivalent with SQUIDs. Therefore, the MI magnetic sensor is the advantages for development very high sensitive and simple structure magnetic sensor. Using their advantages, the MI sensors are used handheld electrical devices, such as electronic compass and motion control sensor for cell phones (Fig. 2. 6).

Based on the literature review, I could classified magnetic sensors according to sensitivity and application [7]–[9]. It represented in figure 2.7.

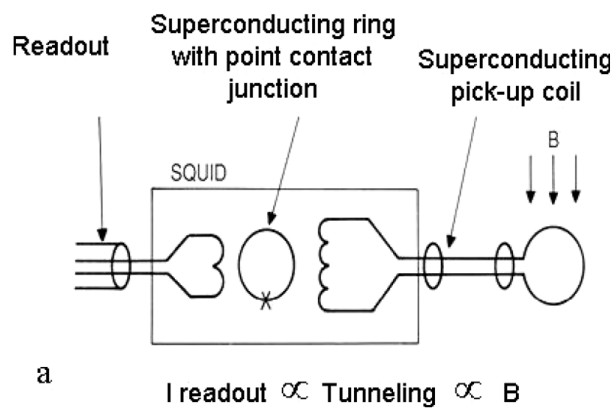


Figure 2.4 Schematic of SQUID

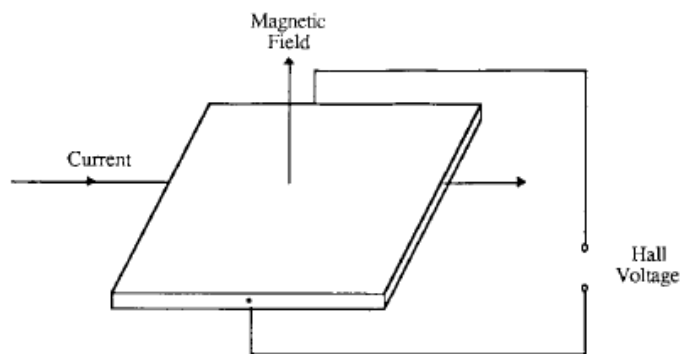


Figure 2.5 Schematic of Hall effect sensors

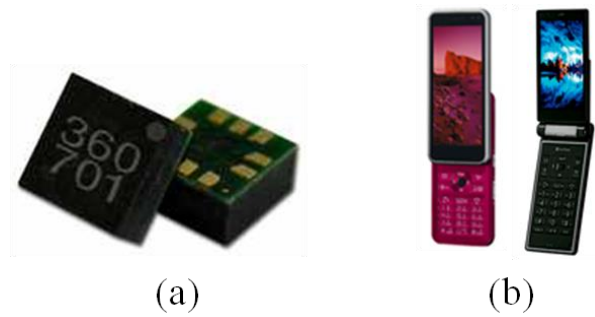


Figure 2.6 Application of MI sensors (a) Electrical compass (b) Motion control sensor for cell phone

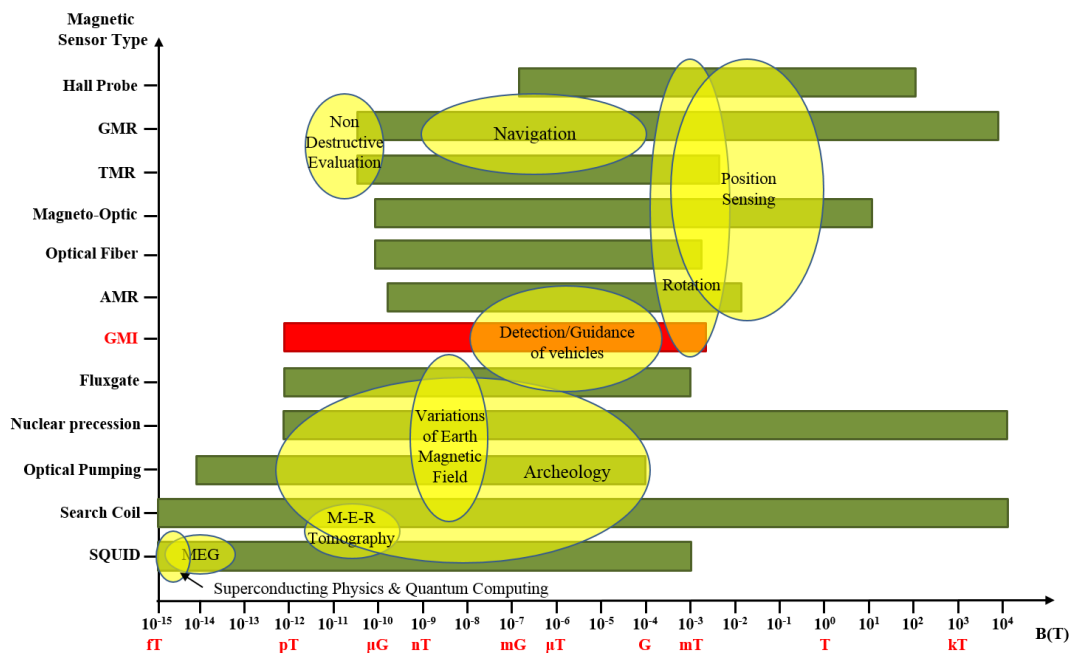


Figure 2.7 A summary of the various magnetic sensors sensitivity

2.3 Theory of Giant Magneto-Impedance Effect

Giant magneto-impedance effect is that when a soft ferromagnetic conductor is subjected to an alternating current, a large change in the ac complex impedance of the conductor can be achieved with applying a magnetic field. GMI Effect was introduced by E. P. Harrison and co-workers in 1936 [10]. They explained well about the foundation of the skin effect and change of permeability. After its discovery there are great advances with using new soft magnetic materials, such as nanocrystalline alloys or amorphous.

Generally, it is to be classified into three types in wires, ribbons or single layered thin films and multi-layered thin films. In this chapter the principles and features of each type will be introduced.

2.3.1 GMI in wires

The early GMI sensor element has wire geometry. It was extensively studied by many researchers [11]–[14]. For a high GMI effect, domain wall should be perpendicular to the applying current as shown in figure 2.8 [15]. The current generates an easy axis driving magnetic field. The longitudinal external magnetic field (H_{ex}) suppresses the circular flux changing. Hence, the magnetic permeability decreases rapidly with the H_{ex} . The magnetic anisotropy is induced by inducing strain or stress during the fabrication or heat treatment. Generally, the melt-spinning process has used for fabrication. During the production, the stress is generated by difference rates of quenching in the inner and outer region of the wire. Whereupon there are two different magnetic domain structure – circumferential and length direction domain (See Fig. 2.8).

The impedance of wire is expressed as follows [16],

$$Z \begin{cases} \left(\frac{1}{2}\right) R_{dc} k a J_0(ka) / J_1(ka), & k = \frac{(1-j)}{\delta}, \quad \delta = \sqrt{2\rho / \omega\mu} \\ R_{dc} + j\omega L, & L = \frac{\mu l}{8\pi} \quad \text{for } \delta \gg a \text{ (without skin effect)} \\ \left(\frac{a}{2\sqrt{2\rho}}\right) R_{dc} (1+j) \sqrt{\omega\mu} & \text{for } \delta \ll a \text{ (strong skin effect)} \end{cases}$$

where R_{dc} is the dc resistance, ρ the resistivity, ω the angular frequency of the current, l the length of wire, a the radius of wire, δ the skin depth, and μ the permeability.

As shown these equations, the impedance sensitively changes by application of external magnetic field utilizing the skin effect and its permeability.

Wire type MI element can be easily fabricated however there are disadvantage for miniaturization and embedment.

2.3.2 GMI in ribbons or single layered thin films

To overcome the problems of wire type elements, single layered thin film geometry has proposed [17]–[21]. The case of sputtered films has advantages in size reduction and patterning. However, there is no different of sensitivity compared with wire case.

When the ac current passes through the thin film, it produced magnetic field which is perpendicular to the direction of ac current. The domain wall movement is suppressed and rotation of magnetization is occurred according to applying external magnetic field along the longitudinal direction. The permeability of the element decreases during this process. As the result, the impedance is changed.

2.3.3 GMI in multi-layered thin films

Lately, the multi-layered thin films structure was reported [22]–[29]. It consists of a conductive layer and two soft ferromagnetic layers as shown in Fig. 2. 10. AC current passes through the conductive layer and it generates magnetic flux in the neighboring magnetic layer. As the result, more uniform magnetic field can be achieved in multi-layered structure. Besides, very high impedance change can be obtained due to sufficiently large difference of resistivity between conductive and magnetic layer.

In this structure, the transverse magnetic anisotropy is suitable to obtain high GMI effect. Figure 2.11 shows that how the permeability is changed by external magnetic field in multi-layered thin film and the relationship between impedance and permeability. When the external magnetic field (H_{ex}) is zero, it has the lowest transverse permeability with transverse magnetic anisotropy as shown in Fig. 2.11(a). At this time, impedance is also the smallest. According to applying external magnetic field in length direction, the direction of magnetization rotates from transverse to longitudinal direction (See Fig. 2.11(b)). During this process, the transverse permeability increases. The increase in permeability is progressed until the external magnetic field reaches at anisotropy field of magnetic layer as shown in the Fig. 2.11(c). At this time, the permeability and impedance reaches maximum value.

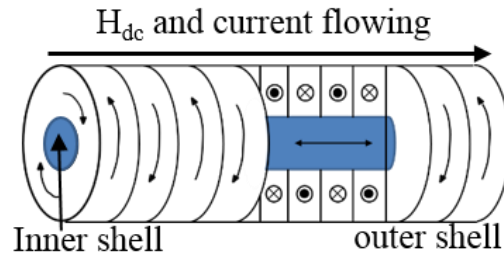


Figure 2.8 Wire type MI sensor element with domain structure

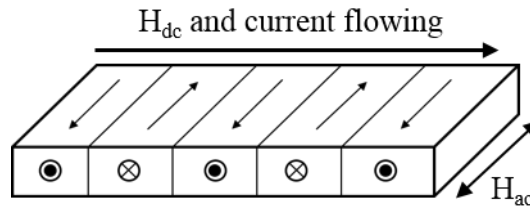


Figure 2.9 Ribbon type MI sensor element with domain structure

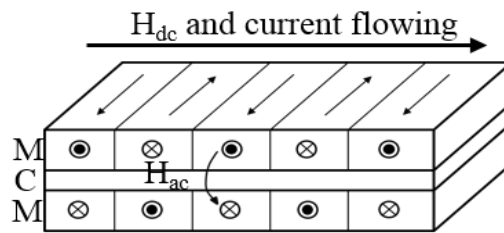


Figure 2.10 Multi-layered type MI sensor element with domain structure

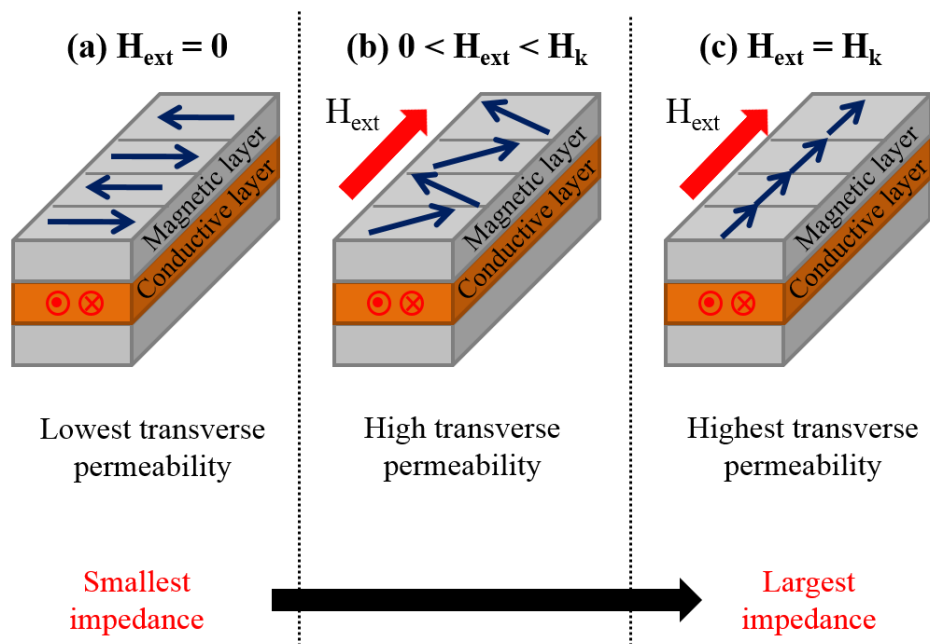


Figure 2.11 A relationship between direction of magnetic anisotropy and permeability in multi-layered thin film structure

References

- [1] J. Lenz, and S. Edelstein, “Magnetic Sensors and Their Application,” *IEEE Sens. Jour.*, **6**, 631-649, 2006.
- [2] P. Brauer, T. Risbo, J.M.G. Merayo, and O.V. Nielsen, “Fluxgate sensor for the vector magnetometer onboard the ‘Astrid-2’ satellite,” *Sens. Actuators A.*, **81**, 184-188, 2000.
- [3] O.V. Nielsen, P. Brauer, F. Primdahl, T. Risbo, J.L. Jorgensen, C. Bee, M. Deyerler, and S. Bauereisen, “A high-precision triaxial fluxgate sensor for space applications: layout and choice of materials,” *Sens. Actuators A.*, **59**, 168-176, 1997.
- [4] J.Vrba and S. E. Robinson, “SQUID sensor array configurations for magnetoencephalography applications,” *Supercond. Sci. Technol.*, **15**, R51–R89, 2002.
- [5] S. Lau, R. Eichardt, L. D. Rienzo, and J. Haueisen, “Tabu Search Optimization of Magnetic Sensor Systems for Magnetocardiography,” *IEEE Trans. Magn.*, **44**, 1442-1445, 2008.
- [6] Y. Murayama, T. Ozawa, S. Yabukami, K. Ishiyama, and K.I. Arai, “High-Frequency Carrier-Type Magnetic Field Sensor with a Sub-pT Resolution Using a Magnetic Film and a Transmission Line,” *J. Magn. Soc. Jpn*, **31**, 17-22, 2007.
- [7] Marina Diaz-Michelena, “Small Magnetic Sensors for Space Applications,” *Sensors*, **9(4)**, 2271-2288, 2009.
- [8] Pavel Ripka, “*Magnetic sensors and magnetometers*,” ISBN: 1-58053-057-5,

2001.

- [9] Slawomir Tumanski, “*Handbook of magnetic measurements*,” ISBN: 978-1-4398-2951-6, 2011.
- [10] E. P. Harrison, G. L. Turney, H. Rowe and H. Gollop, “The Electrical Properties of High Permeability Wires Carrying Alternating Current,” *CLVII Royal Soc. Proc.*, 451, 1936.
- [11] M. Vazquez, “Giant magneto-impedance in soft magnetic “wires,”” *J. Mag. Mag. Mat.*, **226-260**, 693-699, 2001.
- [12] D. Garcia, G. V. Kurlyandskaya, M. Vazquez, F. I. Toth, and L. K. Varga, “Influence of field annealing on the hysteretic behavior of the giant magneto-impedance effect of Cu wires covered with Ni₈₀Fe₂₀ outer shells,” *J. Mag. Mag. Mat.*, **203**, 208-210, 1999.
- [13] K. R. Pirota, L. Kraus, H. Chiriac, and M. Knobel, “Magnetic properties and giant magnetoimpedance in a CoFeSiB glass-covered microwire,” *J. Mag. Mag. Mat.*, **221**, 243-247, 2000.
- [14] R. S. Beach, N. Smith, C. L. Platt, F. Jeffers, and A. E. Berkowitz, “Magnetoimpedance effect in NiFe plated wire,” *Appl. Phys. Lett.*, **68**, 2753, 1996.
- [15] L. V. Panina, K. Mohri, K. Bushida, and M. Noda, “Giant magnetoimpedance and magnetoinductive effects in amorphous alloys (invited),” *J. Appl. Phys.*, **76**, 6198, 1994.
- [16] K. Mohri, T. Uchiyama, L. P. Shen, C. M. Cai, and L. V. Panina, “Sensitive micro magnetic sensor family utilizing magneto-impedance (MI) and stress-impedance (SI) effects for intelligent measurements and controls,” *Sens. Actuators A.*, **91**, 85-90, 2001.

- [17] C. G. Kim, K. J. Jang, H. C. Kim and S. S. Yoon, "Asymmetric giant magnetoimpedance in field-annealed Co-based amorphous ribbon," *J. Appl. Phys.*, **85**, 5447, 1999.
- [18] H. B. Nle, A. B. Pakhomov, X. Yan, X. X. Zhang, and M. Knobel, "Giant magnetoimpedance in crystalline Mumetla," *Solid State Comm.*, **112**, 285-289, 1999.
- [19] G. V. Kurlyandskaya, V. M. Prida, B. Hernando, J. D. Santos, M. L. Sanchez, and M. Tejedor, "GMI sensitive element based on commercial Vitrovac ® amorphous ribbon," *Sens. Actuators A.*, **110**, 228-231, 2004.
- [20] H. Q. Guo, H. Kronmuller, T. Dragon, Z. H. Gheng, and B. G. Shen, "Influence of nanocrystallization on the evolution of domain patterns and the magnetoimpedance effect in amorphous $\text{Fe}_{73.5}\text{Cu}_1\text{Nb}_3\text{Si}_{13.5}\text{B}_9$ ribbons," *J. Appl. Phys.*, **89**, 514, 2001.
- [21] M. Tejedor, B. Hernando, M. L. Sanchez, V. M. Prida, J. M. Garcia-Beneytez M. Vazquez, and G. Herzer, "Magneoimpedance effect in zero magnetostriction nanocrystalline $\text{Fe}_{73.5}\text{Cu}_1\text{Nb}_3\text{Si}_{16.5}\text{B}_6$ ribbons", *J. Mag. Mag. Mat.*, **185**, 61-65, 1998.
- [22] K. Hika, L. V. Panina, and K. Mohri, "Magneto-Impedance in Sandwich Film for Magnetic Sensor Heads," *IEEE Trans. Magn.*, **32**, 4594-4596, 1996.
- [23] T. Morikawa, Y. Nishibe, H. Yamadera, Y. Nonomura, M. Takeuchi, J. Sakata, and Y. Taga, "Enhancement of Giant Magneto-Impedance in Layered Film by Insulator Seperation," *IEEE Trans. Magn.*, **32**, 4965-4967, 1996.
- [24] D. de Cos, L. V. Panina, N. Fry, I. Orue, A. Garcia-Arribas, and J. M. Barandiaran, "Magnetoimpedance in Narrow NiFe/Au/NiFe Multilayer Film

Systems,” *IEEE Trans. Magn.*, **41**, 3697-3699, 2005.

- [25] A. V. Svalov, E. Fernandez, A. Garcia-Arribas, J. Alonso, M. L. Fdez-Gubieda, and G. V. Kurlyanskaya, “FeNi-Based magnetoimpedance multilayers: Tailoring of the softness by magnetic spacers,” *Appl. Phys. Lett.*, **100**, 162410, 2012.
- [26] S. Iida, D. Suzuki, S. Kambe, and O. Ishii, “Enhancement in the Magneto-Impedance (MI) Effect of Multi-Ribbon,” *IEEE Trans. Magn.*, **36**, 3661-3663, 2000.
- [27] M. A. Correa, A. D. C. Viegas, R. B. da Silva, A. M. H. de Andrade, and R. L. Sommer, “Magnetoimpedance of single and multilayered FeCuNbSiB films in frequencies up to 1.8 GHz,” *J. Appl. Phys.*, **101**, 043905, 2007.
- [28] B. Kaviraj, and F. Alves, “Giant magneto-impedance in stress-annealed finemet/copper/finemet-based trilayer structures,” *Physica B*, **403**, 1937-1941, 2008.
- [29] G. V. Kurlyanskaya, L. Elebaile, F. Alves, B. Ahamada, R. Barrue, A. V. Svalov, and V. O. Vas’kovskiy, “Domain structure and magnetization process of a giant magnetoimpedance geometry FeNi/Cu/FeNi(Cu)FeNi/Cu/FeNi sensitive element,” *J. Phys.:condens. Matter*, **16**, 6561-6568, 2004.

Chapter 3

Inducing and Controlling Mechanism of Magnetic Anisotropy

3.1 Introduction

Magnetic field sensors are used in various applications, such as current sensors [1], [2], magnetic compasses [3], [4], and magnetic recording devices [5], as well as in bio-signal sensing [6], [7]. As their use increases, so the more the sensors require higher sensitivity and reliability. Among these sensors, high-frequency carrier-type thin-film sensors (Magneto-Impedance (MI) sensors) are used due to their high sensitivity, ease of miniaturization, quick response and low power consumption [8], [9]. The MI effect is a phenomenon whereby a high-frequency carrier current applied to the thin-film with an external magnetic field, causes significant changes in the permeability of the MI sensors. According to changes in permeability, impedance is changed by the skin effect [10], as shown in Eq. (3.1):

$$Z = \frac{V}{I} = \frac{k\rho l}{2w} \coth\left(\frac{kt}{2}\right) , \quad (k = \frac{1+j}{\delta}, \delta = \sqrt{\frac{2\rho}{\omega\mu}}) \quad (3.1)$$

where

t , w , and l are the thickness, width, and length of the thin film, respectively, δ is the skin depth, ρ is the resistivity, ω is the angular frequency, and μ is the permeability of the conductive layer. As the Eq. (3.1), significantly high changes in impedance can be realized by large variation of permeability. Then, to obtain significant permeability change for the high sensitivity in the sandwich thin film structure, well induced along the transverse direction of in-plane uniaxial magnetic anisotropy is requirement as shown in Fig. 3.1. However, it is difficult to control the uniaxial anisotropy due to the large demagnetization field caused by the magnetic shape anisotropy. To overcome this problem, several methods have been proposed, such as deposition in the magnetic field [11], annealing with bias stress [12], and annealing under a static magnetic field. The anisotropy can be controlled by these methods. Nevertheless, they involve complicated processes or additional equipment that generates a bias stress. Therefore, I have proposed simpler, effective inducing methods for transverse uniaxial magnetic anisotropy.

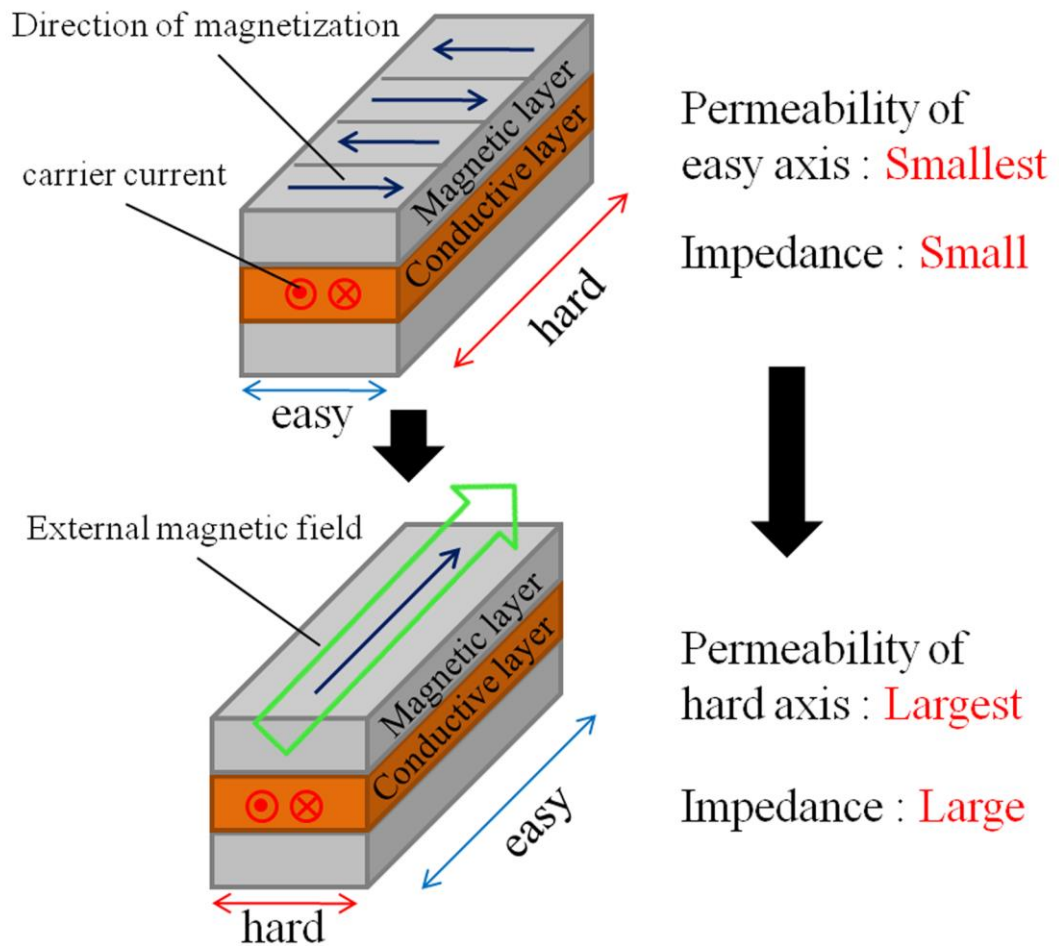


Figure 3.1 The configuration of the change of the permeability according to apply the external magnetic field and carrier current

3.2 Methodology of Direction Control of In-plane Uniaxial Magnetic Anisotropy

In this study, a new control method for anisotropy direction is introduced using inverse-magnetostriction with residual stress, which is generated by the difference in thermal expansion coefficients between the magnetic and conductive layers in the thin film.

The inverse-magnetostriction effect is the change in anisotropy direction of a material when subjected to a mechanical stress, as shown in Fig. 3.2.

The thin film consists of a magnetic layer and a conductive layer. In the case of a multilayer structure, the direction of bending is determined by the combination of the thermal expansion coefficients between the layers, as shown in Fig. 3.3. The two types of bending can be obtained by the appropriate combination of thermal expansion coefficients during the cooling.

First, when the thermal expansion coefficient of the upper layer is larger than that of the lower layer, the thin film bends upwards, as shown in Fig. 3.3 (a). On the other hand, when the thermal expansion coefficient of the upper layer is smaller than that of the lower layer, the bending shown in Fig. 3.3 (b) is generated.

Using the residual stress that is generated by the difference in thermal expansion coefficients between the magnetic and conductive layers, I can control the direction of anisotropy in the magnetic layer of a magnetostrictive material. $\text{Fe}_{72}\text{Si}_{14}\text{B}_{14}$ was used for the magnetic layer, as this is a soft and magnetostrictive material. Therefore, the direction of anisotropy in the $\text{Fe}_{72}\text{Si}_{14}\text{B}_{14}$ thin film can be controlled according to the direction of residual stress by inverse-magnetostrictive effect.

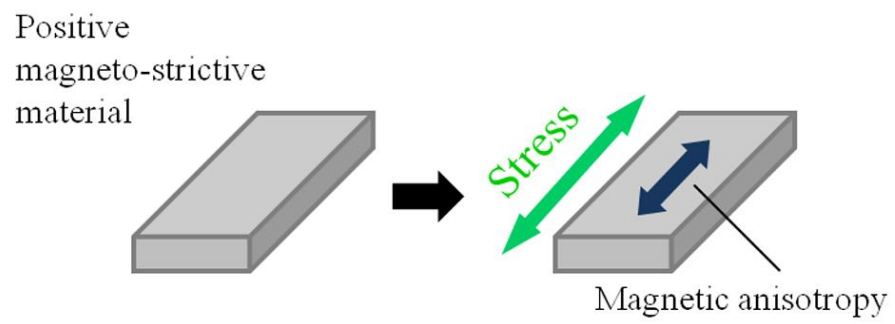


Figure 3.2 Principle of Inverse-Magnetostriction

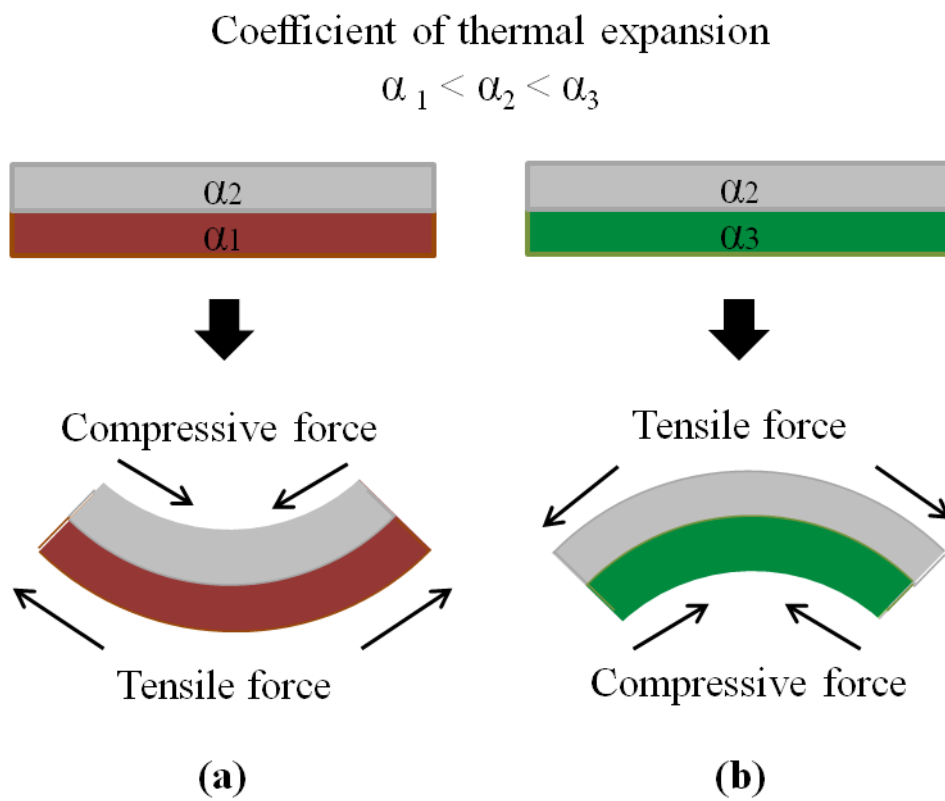


Figure 3.3 Bending direction in the multilayer structure according to changes in the combination of thermal expansion coefficients between layers

As I mentioned above, I use the difference of thermal expansion coefficient between magnetic and conductive layer (see Fig. 3.4) for control of the residual stress in $\text{Fe}_{72}\text{Si}_{14}\text{B}_{14}$ magnetostrictive thin film.

First of all, I assume the two conditions; first, the local stress in the magnetic layer which was induced during deposition is released at 360°C . Second, the anisotropy is induced under the cooling process. During the cooling process (360°C to room temperature), metals shrink. When the materials shrink, inner compressive force (F_{sx}, F_{sy}) is produced in the material then the force generates inner stress (S_{sx}, S_{sy}). The stress (S_{sx}) is perpendicular to inner force (F_{sx}) and its direction is inside to outside, as shown in Fig. 3.5.

The total inner force is divided into the two forces. One is compressive force (shrinkage force) according to material characteristic and the other is bending force according to difference of thermal expansion coefficient between magnetic and conductive layer, as shown in Fig. 3.6 (a) and (c). In addition, the bending force is divided into compressive and tensile forces.

When the thermal expansion coefficient of conductive layer is smaller than magnetic layer, the compressive bending force is generated, as shown in Fig. 3.6 (b). The tensile force is generated when the thermal expansion coefficient of conductive layer is larger than magnetic layer, as shown in Fig. 3.6 (d). After all, when the conductive and the magnetic layer is Mo and $\text{Fe}_{72}\text{Si}_{14}\text{B}_{14}$, respectively, inner force generates the shrinkage and compressive bending force. Therefore, the total inner stress appears in the magnetic layer. At this time, the strength of stress in width direction differs from the strength of the stress in longitudinal direction because the structure of thin film is a rectangular.

Therefore, magnetic anisotropy will be induced in width direction by the inverse-magnetostrictive effect.

By contract, when the thermal expansion coefficient of conductive layer is larger than magnetic layer, inner force in the magnetic layer is composed of shrinkage and tensile forces. In this structure, the direction of shrinkage force is opposite to the direction of bending (tensile) force. Thus, I cannot expect the direction of sum of the two forces. Therefore, to analyze this case, it needs to carry out simulations and experiments.

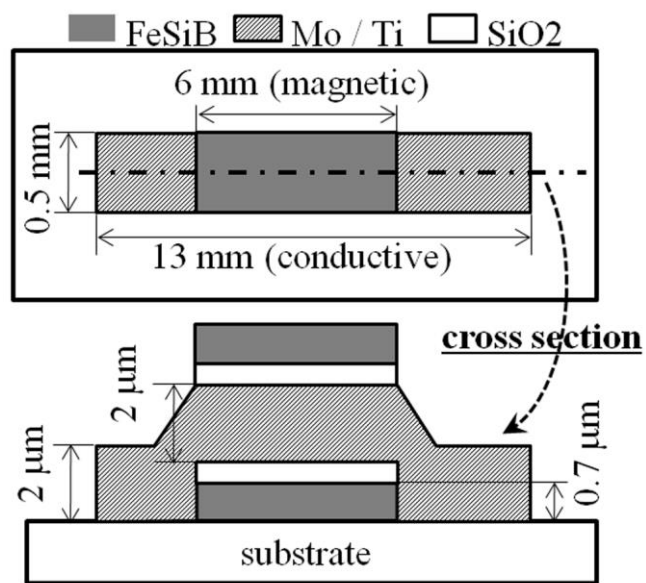


Figure 3.4 A configuration of deposited thin-film: The fabricated thin-films consist of magnetic layer and conductive layer. $\text{Fe}_{72}\text{Si}_{14}\text{B}_{14}$ was used for magnetic layer. Molybdenum and titanium were used for conductive layer

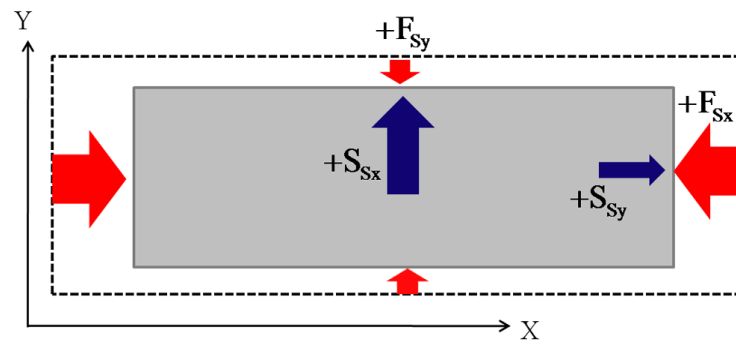


Figure 3.5 A relationship between inner force and residual stress in the rectangular shape: $+F_s$ denotes the inner compressive (shrink) force. S_{sx} denotes the residual stress by inner (compressive) force ($+F_{sx}$). S_{sy} denotes the residual stress by inner (compressive) force ($+F_{sy}$)

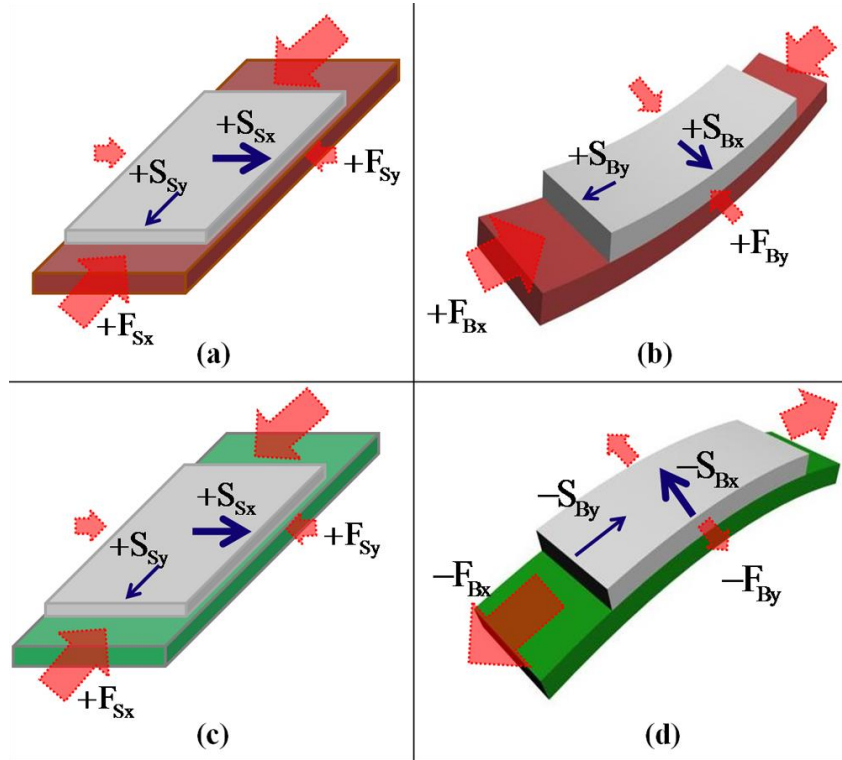


Figure 3.6 Direction of residual stress in the magnetic layer according to direction of inner forces: (a) Direction of shrink force and residual stress by material characteristics. (Conductive layer: Mo). (b) Bending force and residual stress by difference of thermal expansion coefficient between the magnetic layer (FeSiB) and the conductive layer (Mo). (c) Direction of shrink force and residual stress by material characteristics (Conductive layer: Ti). (d) Bending force and residual stress by difference of thermal expansion coefficient the magnetic layer (FeSiB) and the conductive layer (Ti)

3.3 Verification by FEM Simulation

To verify the direction and strength of residual stress, I carried out FEM simulation. I used quarter of the thin film because of the symmetrical structure (see Fig. 3.7). The direction of residual stress in the magnetic layer depends on the materials combination of magnetic and conductive layer. When I used Molybdenum ($5.4 \times 10^{-6} / K^{-1}$) at the conductive layer, the tensile residual stress was generated, and the produced residual stress of the width direction is larger than the longitudinal direction (see Fig. 3.7(a)). Therefore the in-plane uniaxial anisotropy will be induced along the width direction by the residual stress. However, when I used Titanium at the conductive layer, the compressive inner stress of width direction is larger than that of longitudinal direction, as shown in Fig. 3.7(b). It cannot induce the in-plane uniaxial anisotropy along the width direction. In conclusion, using the Molybdenum is suitable for inducing anisotropy in width direction.

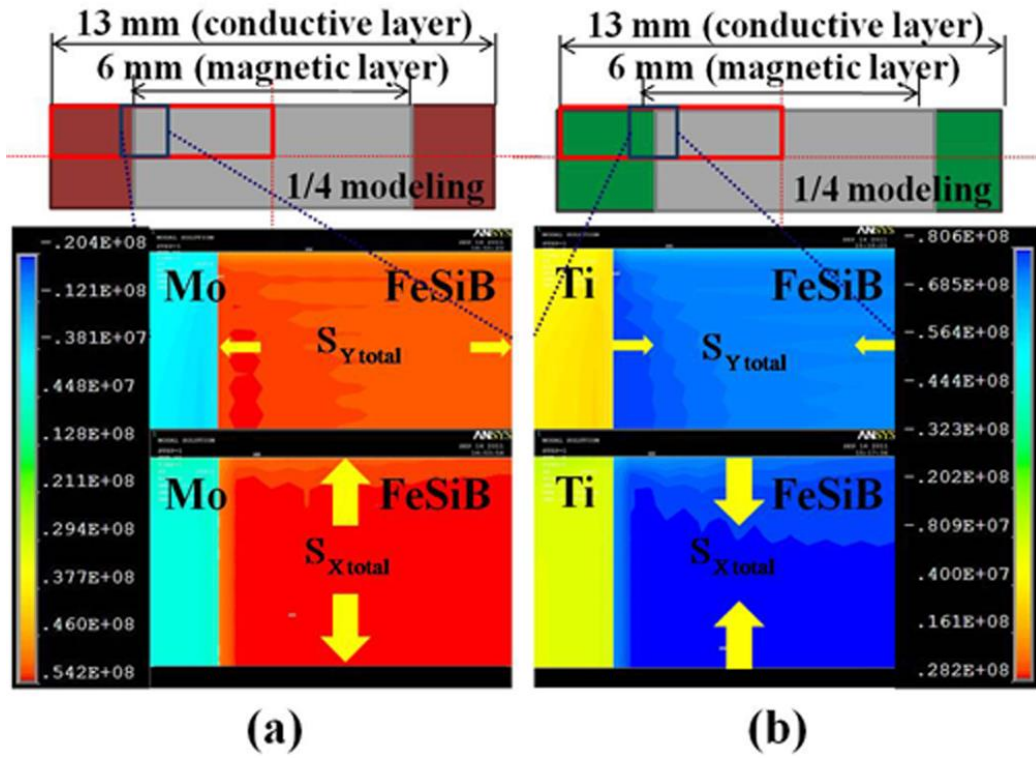


Figure 3.7 FEM simulation of residual stress distribution using quarter model: (a) Direction of residual stress in the magnetic layer (FeSiB) using Mo for conductive layer. (b) Direction of residual stress in the magnetic layer (FeSiB) using Ti for conductive layer. The yellow arrows denote the direction of residual stress and the thickness denotes the strength of the stress

3.4 Fabrication of Thin film

The fabricated thin-films consist of magnetic layer and conductive layer. $\text{Fe}_{72}\text{Si}_{14}\text{B}_{14}$ (coefficient of thermal expansion: $6.5 \times 10^{-6} / K^{-1}$) was used for the magnetic layer. Titanium ($8.3 \times 10^{-6} / K^{-1}$) and molybdenum ($5.4 \times 10^{-6} / K^{-1}$), were used for conductive layer. The concrete properties of materials, which were used expressed in Table. 3.1.

A schematic drawing of the layered thin film is shown in Fig. 3.8. These thin-film layers were deposited by RF sputtering on the cover glass substrate which has 150 μm thickness. The thickness of the magnetic and the conductive layers are 0.7 and 2 μm , respectively, and they are insulated by 0.25 μm thick SiO_2 . The magnetic layer ($\text{Fe}_{72}\text{Si}_{14}\text{B}_{14}$) was deposited in the argon gas pressure 16 mTorr and the sputtering-input power was 100W. The conductive layer (molybdenum and titanium) was deposited in the argon gas pressure 14 mTorr and the sputtering-input power was 100W, as shown in Table 3.2. The lift off method was used for the fabrication (Fig. 3.9). After the fabrication, I annealed the thin-films to release the local stress, which was induced during the deposition, in rotating-field of 0.3T at 360°C in 2 h. The annealing condition is as shown in Figure 3.10.

Table 3.1
The mechanical properties of the target materials

Material	Coefficient of thermal expansion ($10^{-6}/\text{K}^{-1}$)	Young's modulus (/GPa)	Poisson's ratio
FeSiB	6.5	110	0.3
Molybdenum	5.4	324.8	0.32
Titanium	8.3	120.2	0.35

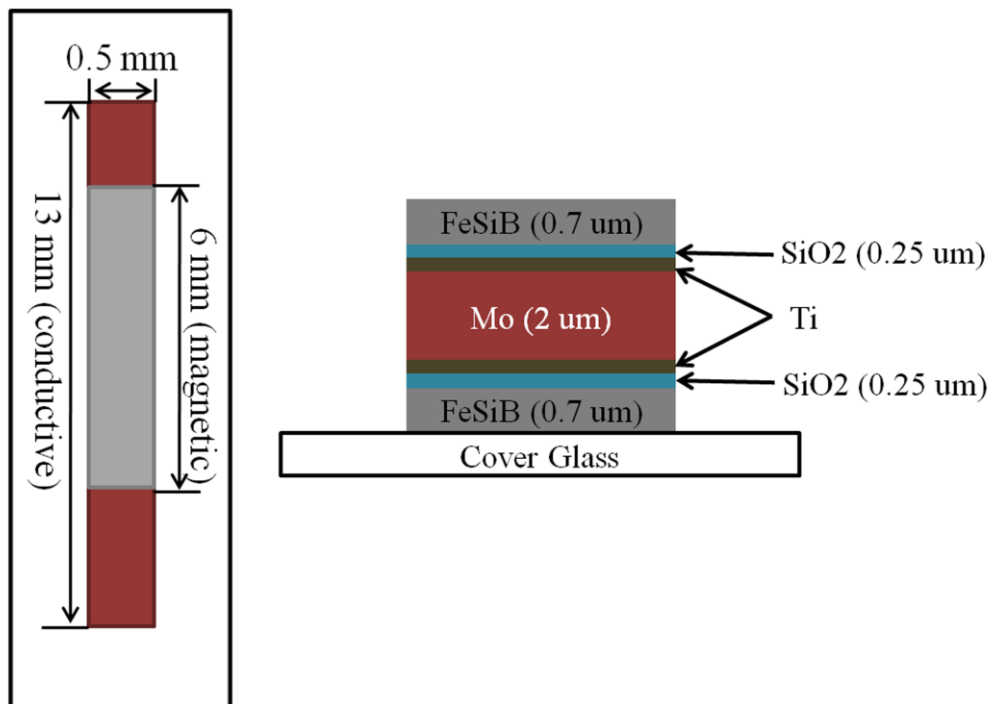


Figure 3.8 A structure and size of the thin film

Table 3.2
Sputtering condition of each material

	FeSiB	SiO ₂	Mo	Ti
ArGas [mTorr]	16	4	14	14
Power [W]	100	150	100	100
Time [min]	70	45	50	85

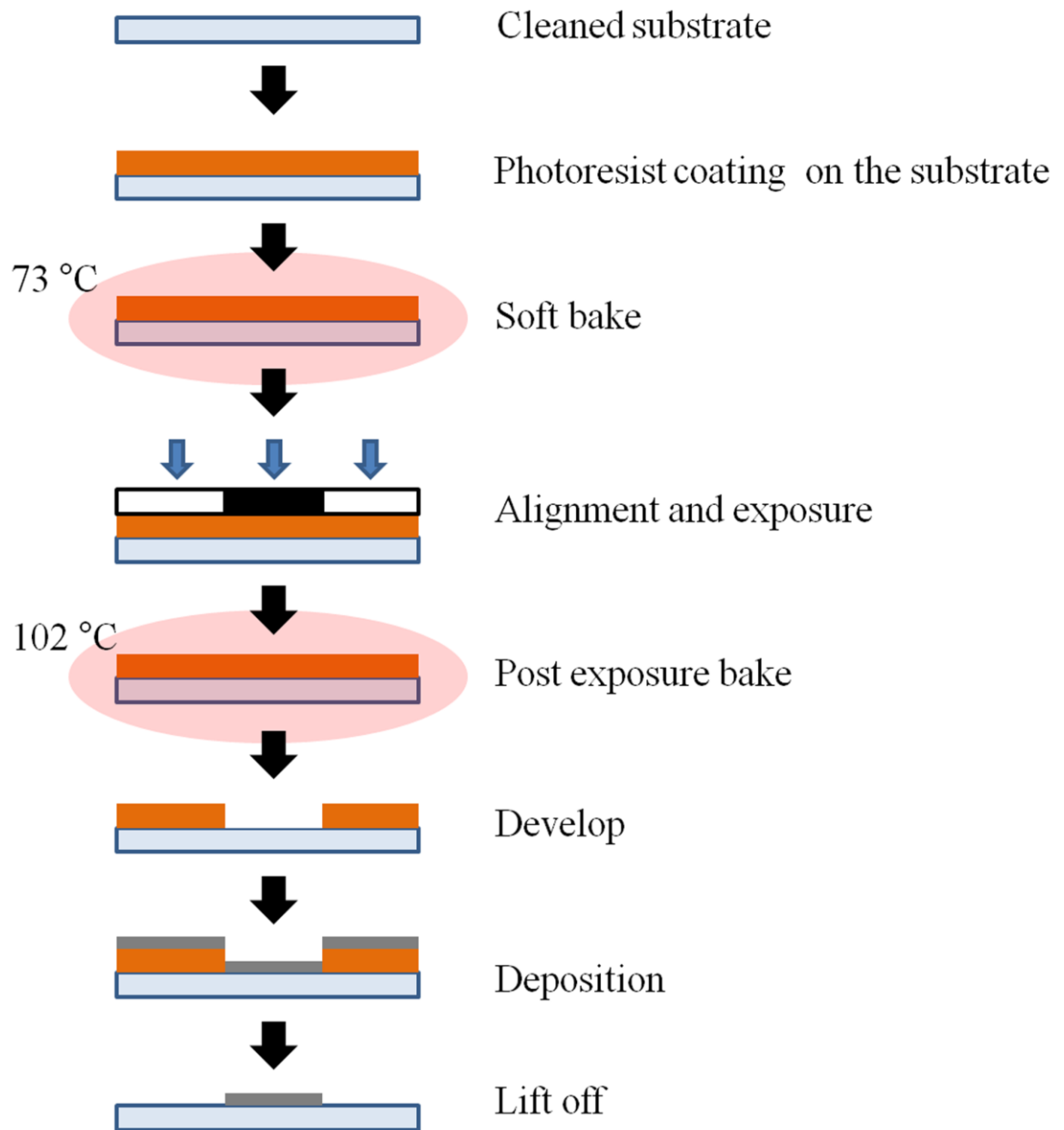


Figure 3.9 A process of the thin film fabrication

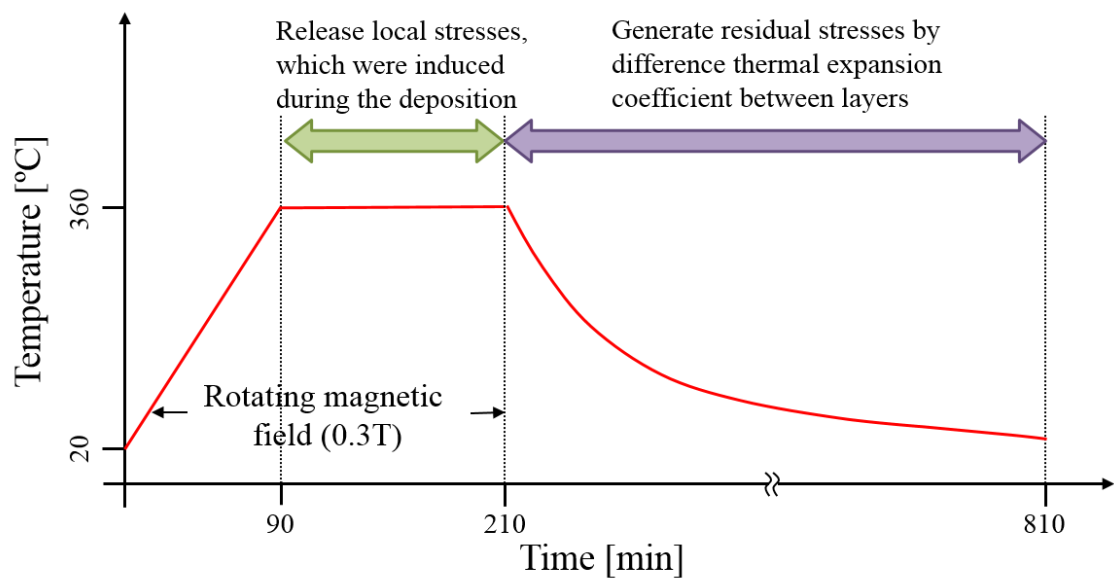


Figure 3.10 Annealing condition

3.5 Experimental Result

The magnetic domain patterns of fabricated thin films were observed by Kerr-microscope. The method of domain observation is that I set the fabricated thin film on the stage of kerr-microscope (NEOARK BH-780IP) and observed in-plane magnetic domain on the magnetic layer by 10 times the lens (Mitutoyo). First, the white light was generated by the mercury lamp power supply (OLYMPUS BH2-RFT-T3). This light was polarized. Then, the reflected light was collected using CCD camera (OLYMPUS U-TV1X-2 & U-CMAD3). The domain observation results were presented contrast distinction according to the direction of anisotropy.

Figure 3.11 shows the induced magnetic domain patterns on the magnetic layer. When the coefficient of thermal expansion of magnetic layer ($\text{Fe}_{72}\text{Si}_{14}\text{B}_{14}$) is larger than conductive layer (Molybdenum), the in-plane uniaxial magnetic anisotropy was induced along the transverse direction by the generated residual stress. This result confirm to my expectation and verification according to the FEM simulation. In contrast, when the coefficient of thermal expansion of magnetic layer ($\text{Fe}_{72}\text{Si}_{14}\text{B}_{14}$) is smaller than conductive layer (Titanium), the transverse direction magnetic anisotropy did not induced in the magnetic layer as shown in Fig. 3.12. The proposed methods with simulation results were verified through the experiments. As the results, direction of the uniaxial magnetic anisotropy could be controlled by difference of thermal expansion coefficient between magnetic and conductive layer.

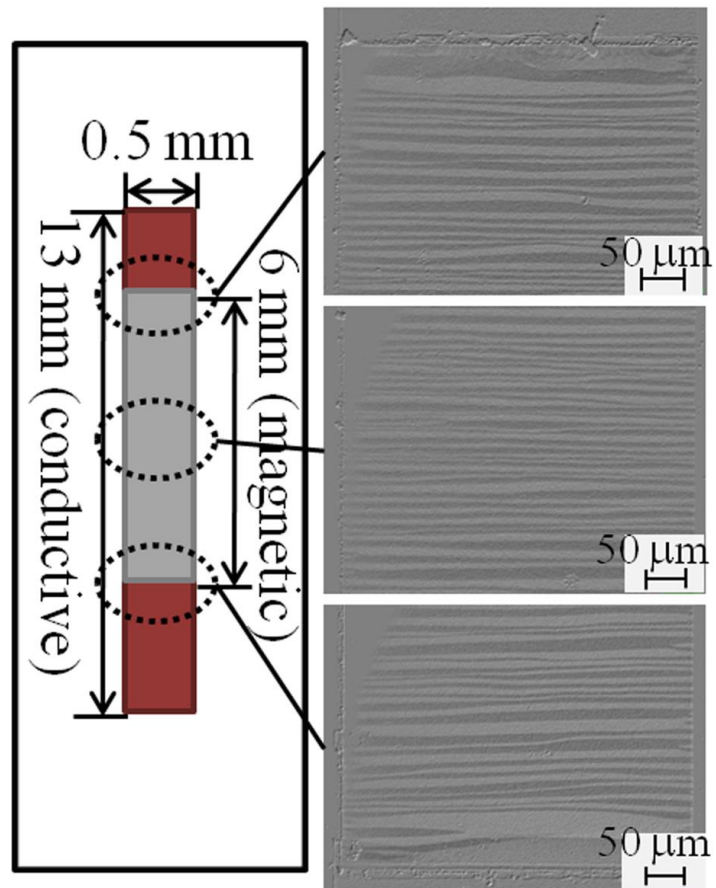


Figure 3.11 A result of the magnetic domain observation in the magnetic layer with Mo conductive layer. FeSiB and Mo were used for magnetic layer and conductive layer, respectively

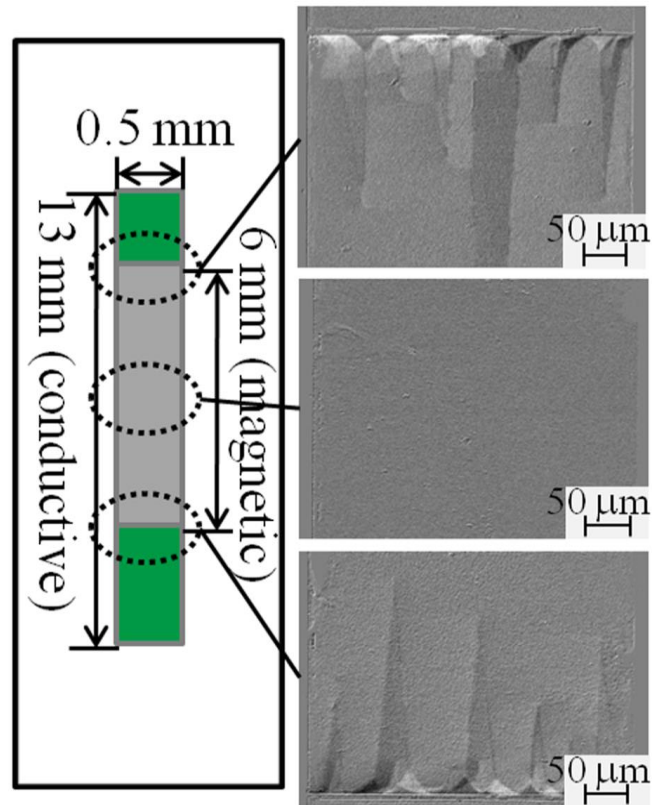


Figure 3.12 A result of the magnetic domain observation in the magnetic layer with Ti conductive layer. FeSiB and Ti were used for magnetic layer and conductive layer, respectively

3.6 Summary

In this chapter, I proposed a new control method of direction of the uniaxial anisotropy along the transverse direction. Through the simulation and experiment results, I could verify the in-plane uniaxial magnetic anisotropy in the transverse direction utilizing the proposed method. Furthermore, I could remove the complicated process or additional equipments using physical phenomenon. Therefore, this work is well worth preliminary research for the high sensitivity sensor. The proposed methods have not yet been reported. My ongoing work is focused on the developing the high sensitivity magnetic sensor based on the proposed control methods.

Condition 1:

Thermal expansion coefficient :

Magnetic layer (FeSiB) > Conductive layer (Mo)

In this case, the well-induced in-plane uniaxial anisotropy along the transverse direction can be induced in the magnetic layer.

Condition 2:

Thermal expansion coefficient :

Magnetic layer (FeSiB) < Conductive layer (Ti)

By contrast, when the thin film was deposited in the condition 2, the in-plane uniaxial anisotropy cannot be induced along the transverse direction as shown in Fig. 3.12. It represents that the control of anisotropy direction depends on the material of conductive layer.

References

- [1] C. Xiao, L. Zhao, T. Asada, W. G. Odendaal, and J. D. van Wyk, "An Overview of Integratable Current Sensor Technologies," *Proc. IEEE Industry Applications Conference, 2003. 38th IAS Annual Meeting*, 1251-1258, 2003.
- [2] J. Pelegri, J. B. Ejea, D. Ramirez, and P. P. Freitas, "Spin-valve current sensor for industrial applications," *Sens. Actuators A.*, **105**, 132-136, 2003.
- [3] M. J. Caruso, "Applications of Magnetic Sensors for Low Cost Compass Systems," *Proc. IEEE Position Location and Navigation Symposium*, 117-184, 2000.
- [4] M. J. Caruso, and L. S. Withanawasam, "Vehicle Detection and Compass Applications using AMR Magnetic Sensors," *Proc. Sensors Expo and Conference*, 1999.
- [5] K. Mohri, T. Kohzawa, K. Kawashima, H. Yoshida, and L. V. Panina, "Magneto-inductive effect (MI effect) in amorphous wires." *IEEE Trans. Magn.*, **28**, 3150-3152, 1992.
- [6] S. Tanaka, Z. Aspanut, H. Kurita, C. Toriyabe, Y. Hatuskade, and S. Katsura, "Bio-application of high-Tc SQUID magnetic sensor," *J. Mag. Mag. Mat.*, **300**, 315-319, 2006.
- [7] D. L. Graham, H. Ferreira, J. Bernardo, P. P. Freitas, and J. M. S. Cabral, "Single magnetic microsphere placement and detection on-chip using current line designs with integrated spin valve sensors: Biotechnological applications," *J. Appl. Phys.*, **91**, 7786, 2002.

- [8] Y. Murayama, T. Ozawa, S. Yabukami, K. Ishiyama, and K.I. Arai, "High-Frequency Carrier-Type Magnetic Field Sensor with a Sub-pT Resolution Using a Magnetic Film and a Transmission Line," *J. Magn. Soc. Jpn*, **31**, 17-22, 2007.
- [9] T. Morikawa, Y. Nishibe, H. Yamadera, Y. Nonomura, M. Takeuchi, and Y. Taga, "Giant Magneto-Impedance Effect in Layered Thin Films," *IEEE Trans. Magn.*, **33**, 4367-4372, 1997.
- [10] L. Panina, and K. Mohri, "Magneto-impedance effect in amorphous wires," *Appl. Phys. Lett.*, **65**, 1189-1191, 1994.
- [11] H. Yamadera, "Sensing of Magnetic Field and Strain utilizing Magneto-Impedance Effect," *IEEJ. Trans. FM*, **129**, 113-116, 2009.
- [12] K. Imamura, K. H. Shin, K. Ishiyama, M. Inoue, and K. I. Arai, "Anisotropy Control of Magnetostrictive Film Patterns," *IEEE Trans. Magn.*, **37**, 2025-2027, 2001.

Chapter 4

Investigation of Magnetic Properties According to Changes in Geometry of Elements

4.1 Introduction

To improve the MI ratio, it is necessary to control the strength of induced magnetic anisotropy [1]-[4]. In addition, investigation of the fabrication condition is required to manufacture the MI sensor [5]. The magnetic anisotropy which has low energy can be reacted and rotated by very small magnetic field. It means that reduction of magnetic anisotropy energy is necessary to develop high sensitive MI sensor element.

Controlling the strength of magnetic anisotropy can be realized by changes in stresses which are generated in magnetic layer. I can produce the different stresses according to changes in geometry of the elements such as thin film's length, width and thickness [6].

The bending which is generated by difference of thermal expansion coefficient between layers is used to induce the magnetic anisotropy. Therefore, the stress in the magnetic layer can be calculated by the beam equation as [7]-[9]:

$$\sigma = \frac{Ed\delta}{3L^2(1-\nu)t} \quad (4.1)$$

where E , ν , d , and L , denote Young's modules, Poisson's ratio, and the thickness, and length of the beam, respectively. t is the film thickness. According to Eq. (4.1), the stress in the thin film can be controlled by changing the length and thickness of the film.

It has relations between stresses and strength of magnetic anisotropy field as follow [10], [11]:

$$E_{me} = \frac{3}{2} \lambda_s \sigma = \frac{1}{2} H_k M_s \quad (4.2)$$

where E_{me} is induced magnetoelastic energy in the magnetic layer. H_k is anisotropy field, M_s is the saturation magnetization. λ_s is the saturation magnetostriction, and σ is the stress in the thin film.

According to the equation of 4.2, small magnetoelastic energy can be achieved by reduction of the produced stress and its small anisotropy field (H_k). Consequently, I examine the changes of H_k values according to changes in the geometrical properties (aspect ratios between length and width and ratios of thickness between magnetic and conductive layer).

4.2 Influence of Ratio of the Thickness on Magnetic Anisotropy

In this chapter, I will introduce the dependence of magnetic anisotropy on the ratio of the thicknesses between the two layers to develop a GMI sensor element with a high, and adjustable, sensitivity. The generated total anisotropy field ($H_{k(t)}$) in the magnetic layer depends on the shape anisotropy ($H_{k(s)}$) and the induced anisotropy ($H_{k(i)}$). For control of the anisotropy field, I change the thickness of the magnetic layer. The $H_{k(s)}$, the $H_{k(i)}$ and the generated bending stresses are numerically analyzed. In addition, the $H_{k(t)}$ is obtained experimentally. Based on this, I investigate the relationship between induced anisotropy and the ratio of thickness.

4.2.1 Calculation of generated stress and shape anisotropy

The shape anisotropy and the bending stress which induces the magnetic anisotropy will be discussed by numerical analysis in this chapter.

Bending Stress

A multi-layer thin film which consisted of magnetic and conductive layers, as shown in Fig. 4.1(a), was used in this study. As I mentioned above, the local stress in the magnetic layer, which was induced during deposition, was released by annealing at 360°C. Then, I cooled the thin film from 360°C to room temperature (about 25°C). During the cooling process, the thin film bends due to the difference of the thermal expansion coefficient between layers (Fig. 4.1(b)). Measuring the bending deformation is difficult because the film is small and thin. Therefore, through a numerical analysis, I estimate the deformation of a thin film and the stress generated in the magnetic layer. The deformation is assumed to along only the longitudinal direction in a rectangular

model.

First, the radius of curvature can be estimated using [12]

$$\frac{1}{\rho} = \frac{6(a_c - a_m)(t - t_0)(1 + m)^2}{h(3(1 + m)^2 + (1 + mn) + (m^2 + \frac{1}{mn}))} \quad (m = \frac{t_m}{t_c}, \quad n = \frac{E_m}{E_c}) \quad (4.3)$$

where t_m , E_m and a_m are the thickness, Young's modulus and the thermal expansion coefficient of the magnetic layer, respectively. t_c , E_c and a_c are the thickness, Young's modulus and the thermal expansion coefficient of the conductive layer, respectively. h denotes the total thickness of the thin film.

According to changes in the thickness of the magnetic layer (from 0.5 μm to 2.5 μm), I examine the variation in the radius of curvature. The stresses generated in the magnetic layer were calculated by using the obtained radius of curvatures. The stress can be expressed as follows:

$$\sigma = -\frac{Ey}{\rho}, \quad (4.4)$$

where σ denotes the stress generated by bending. E , y and ρ are Young's modulus, the vertical distance from the neutral plane and the curvature of the magnetic layer, respectively. For an estimate of the stress, the neutral plane must be estimated. Based on the schematic layout of Figure 4.2, the neutral plane of a thin film can be calculated using [13]

$$t_s' = \frac{E_c t_c^2 - E_m t_m^2}{2(E_c t_c + E_m t_m)} \quad (4.5)$$

where t_s' denotes the distance between the neutral plane and the contact plane of the layer. t_m and E_m are the thickness and the Young's modulus of the magnetic layer, respectively. t_c and E_c are the thickness and the Young's modulus of the conductive layer, respectively. The calculated bending stress, which changes depending on the thickness of magnetic layer, was obtained as shown in Fig. 4.3. As a result, when the magnetic and the conductive layers have equivalent thicknesses, the generated stress is the larger in the magnetic layer. These stresses caused by bending deformation induce a transverse magnetic anisotropy in a magnetostrictive material.

Shape Anisotropy

As I mentioned above, the magnetic anisotropy generated in the magnetic layer is comprised of the induced and the shape anisotropies. Thus, a variation in the shape anisotropy with changing thickness of the magnetic layer is considered in this subsection.

A calculation of the shape anisotropy is impossible for a rectangular model because the demagnetizing factor cannot be calculated [14]. Therefore, I used an ellipsoid model instead of a rectangle. First, the demagnetizing factor of each direction was obtained for each thickness of the magnetic layer. The demagnetizing factor can be estimated as follows [15]:

$$L/4\pi = \frac{c}{a} \left(1 - e^2 \right)^{\frac{1}{2}} \frac{K - E}{e^2}, \quad (4.6)$$

$$M/4\pi = \frac{c}{a} \frac{E - (1-e^2)K}{e^2(1-e^2)^{\frac{1}{2}}}, \quad (4.7)$$

$$N/4\pi = 1 - \frac{cE}{a(1-e^2)^{\frac{1}{2}}}, \quad (4.8)$$

where a , b , and c are the ellipsoid semi-axes. L , M , and N are the demagnetizing factors which correspond to the semi-axes a , b , and c , respectively. K and E are complete elliptic integrals whose arguments are

$$e = (1 - b^2/a^2)^{\frac{1}{2}}. \quad (4.9)$$

When the rectangular model is used instead of an ellipsoid, a and b become 1×10^{-3} and 0.5×10^{-3} because the dimension of the rectangular thin film is $1 \text{ mm} \times 2 \text{ mm}$. The results for the shape anisotropy for various thickness of the magnetic layer are shown in Fig 4.4. The shape anisotropy increases because the demagnetizing field in the thickness direction (direction of c) is decreased by increasing thickness.

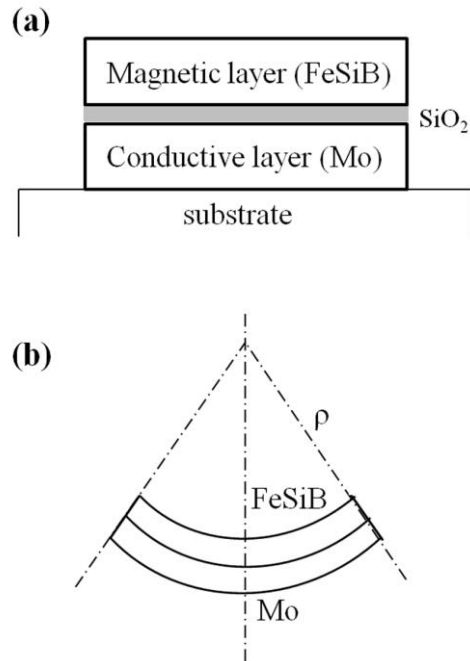


Figure 4.1 (a) Thin film structure. (b) Positive bending caused by the different thermal expansion coefficients under cooling

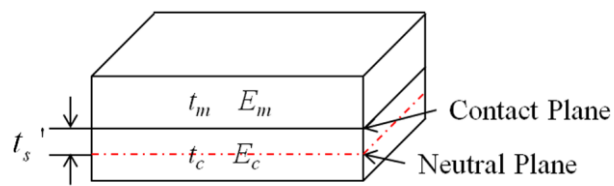


Figure 4.2 Neutral plane between the two deposited layers. The dotted line denotes the neutral plane

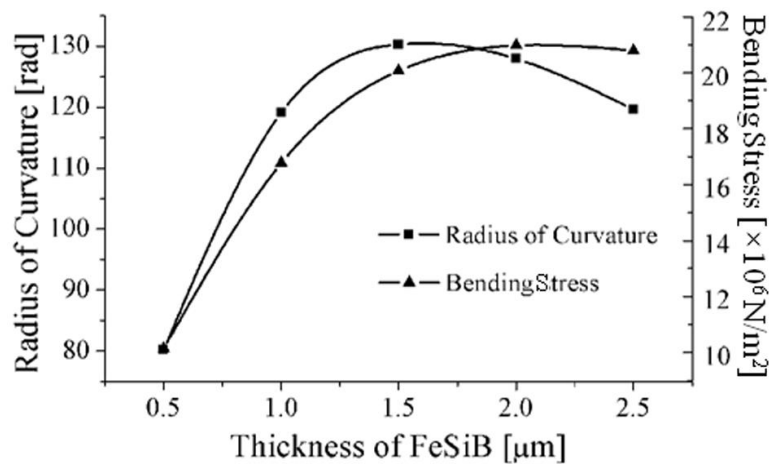


Figure 4.3 Calculation results: radius of curvature and bending stress

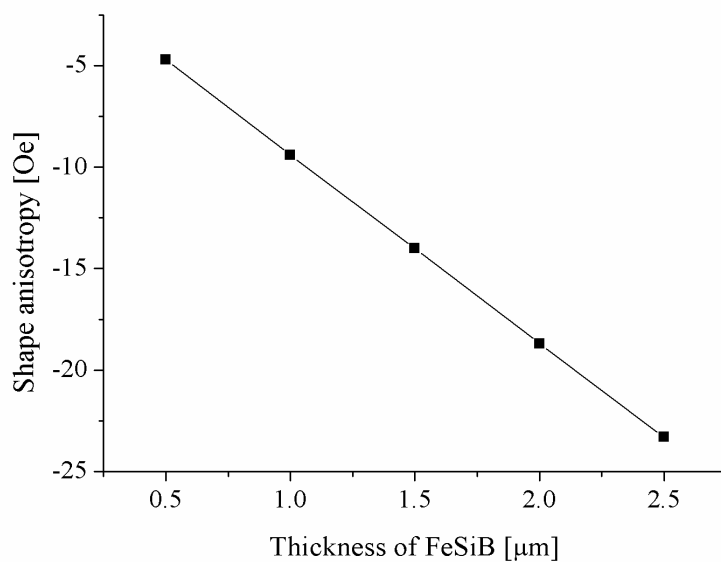


Figure 4.4 Calculated shape magnetic anisotropy for various thicknesses of the magnetic layer

4.2.2 Experimental analysis

To verify the relationship between $H_{k(t)}$ and the magnetic layer's thickness, I fabricated thin films that consisted of magnetic and conductive layers. $Fe_{72}Si_{14}B_{14}$ and molybdenum were used for the magnetic and the conductive layers, respectively. The dimensions of the fabricated thin film were $1\text{ mm} \times 2\text{ mm}$. The thickness of the conductive layer was fixed at $2\text{ }\mu\text{m}$, and I increased the magnetic layer's thickness from $0.5\text{ }\mu\text{m}$ to $2.5\text{ }\mu\text{m}$ as shown in Fig. 4.5. The thin films were fabricated slide glass substrates of 1 mm in thickness by using RF magnetron sputtering and the two layers were insulated by using SiO_2 of $0.25\text{ }\mu\text{m}$ in thickness. I assumed that the two layers (Mo / FeSiB layer) were glued tightly by sputtering. There was a SiO_2 insulator between the two layers. The SiO_2 has a relatively low Young's modulus (73 Gpa) composed to Mo (324 Gpa) and FeSiB (118 Gpa). Therefore, the generated stress can be applied to the magnetic layer. For these reasons, in this study, I neglected the interface effect.

The induced transverse magnetic anisotropy (magnetic domain) was observed by using a Kerr microscope. Figure 4.5 shows the results of the domain observation. I measured the variation of $H_{k(t)}$ according to changes in the ratio of the thicknesses of the two layers by using a vibrating sample magnetometer (VSM). The $H_{k(t)}$ value can be determined based on the difference between the width and the length axes. With increasing of magnetic-layer thickness, the slope of the width axis becomes gentle, as shown in Fig. 4.6. Based on the VSM results, the $H_{k(t)}$ was obtained, as shown in Fig 4.7, and it changed from width easy to length easy, which was the result of a combination of the shape and the induced anisotropies.

As the experimental results, The generated magnetic anisotropy ($H_{k(t)}$) was determined by using the shape ($H_{k(s)}$) and the induced ($H_{k(i)}$) anisotropies. According

changes in the ratio of the thickness, the neutral plane which has stress free was changed. As the result, different amount of stress was produced in the magnetic layer by the different thickness ratio.

However, the $H_{k(i)}$ is the major factor to decide $H_{k(t)}$, as shown in Fig. 4.8. The $H_{k(i)}$ has an intimate relationship with the bending stress generated by the difference in the thermal expansion coefficients between the two layers. Thus, I numerically calculated the amount of bending stress for various thicknesses of the magnetic layer. These variations of the bending stresses influence the induced anisotropy ($H_{k(i)}$), and the $H_{k(i)}$ is inversely proportional to the bending stress, as shown in Fig. 4.9.

Consequently, the ratio of the thicknesses between the magnetic and the conductive layers is a very important factor in deciding the magnetic anisotropy for our proposed method to control the magnetic anisotropy.

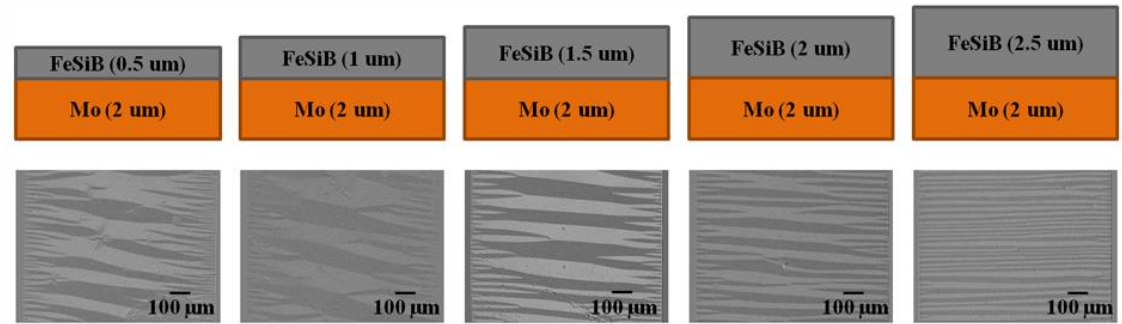


Figure 4.5 Schematic of the fabricated thin films and their observed domains for various thicknesses of the magnetic layer

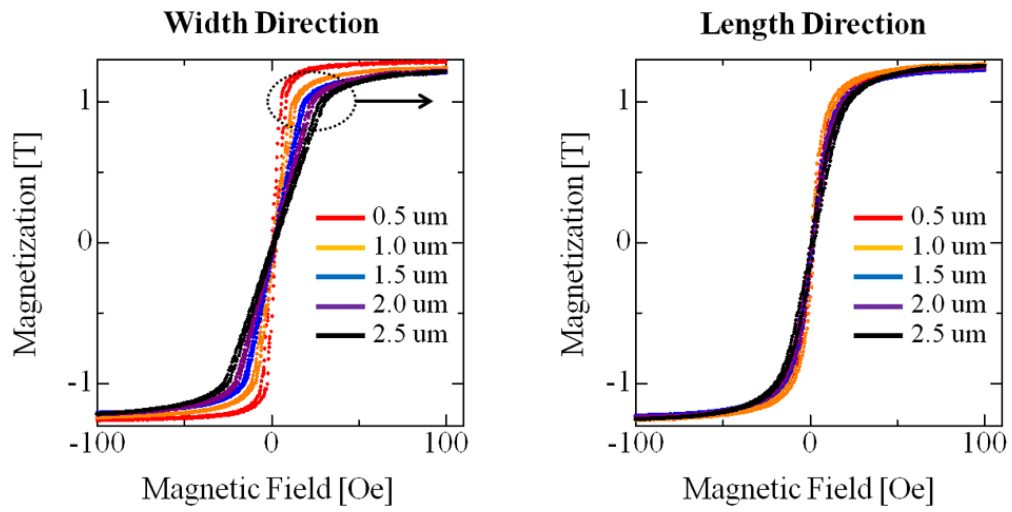


Figure 4.6 VSM measurement results for the Hk Total between the width and the length direction

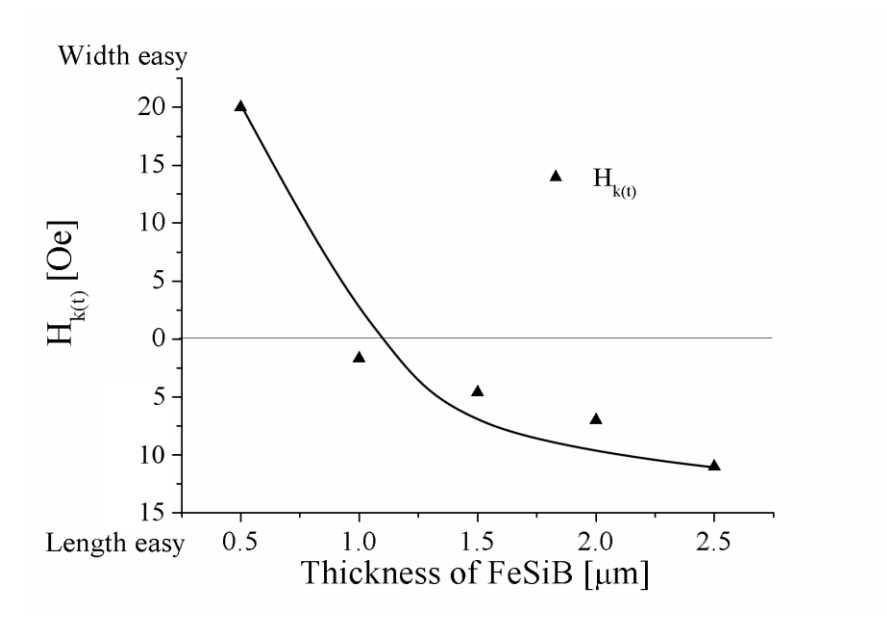


Figure 4.7 $H_{k(t)}$ result obtained from VSM measurements

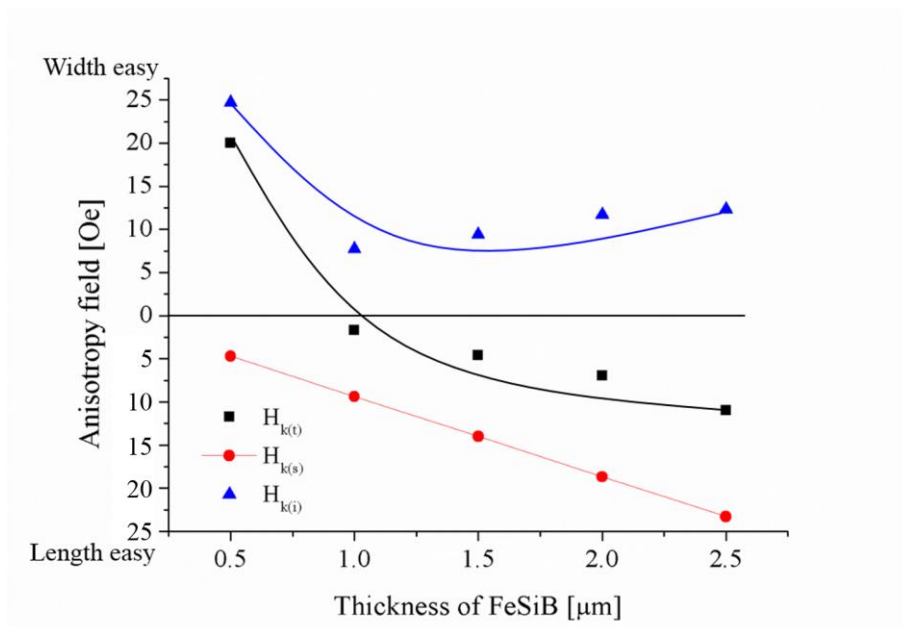


Figure 4.8 Analysis of the magnetic anisotropy: $H_{k(t)}$, $H_{k(s)}$, and $H_{k(i)}$

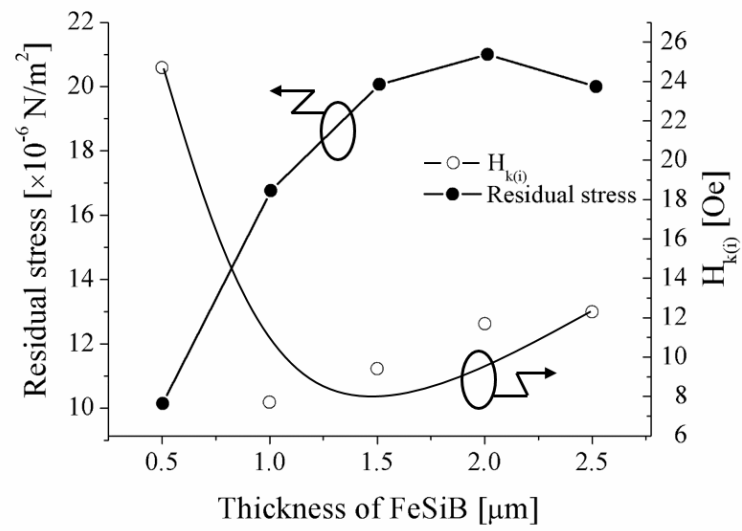


Figure 4.9 Relationship between bending stress and induced magnetic anisotropy

4.3 Influence of Width of Magnetic Layer on Magnetic Anisotropy

In this chapter, I will introduce how the induced anisotropy field varies by the width of magnetic layer. The thickness of magnetic and conductive layer is fixed. It also one of the method to induce magnetic anisotropy which has a relatively lower magnetoelastic energy for improve of MI effect.

4.3.1 Fabrication of the elements

The elements for the experiments were prepared as shown in Fig. 4.10. The thickness of the conductive layer was 1.4 μm . FeSiB positive magnetostrictive material was deposited in 0.7 μm thick on the conductive layer. The magnetic and conductive layers were insulated with a SiO_2 layer.

The width of the sensor was changed from 40 μm to 800 μm . The fabricated sensors were annealed with a rotating magnetic field (0.3 T) at 360°C. After fabricating the sensor, I carried out observation of the magnetic domain by Kerr-effect microscopy and magnetization curves obtained using a vibrating sample magnetometer (VSM).

4.3.2 Experimental results according to changes in width of the magnetic layer

First of all, I carried out observation of magnetic domain using the 40 μm , and 50 μm width samples at a length of 4mm. It is difficult to induce magnetic anisotropy against large demagnetizing field in very narrow width element. As shown in domain observation results (see Fig. 4.11), the uniform magnetic anisotropy could be induced along the transverse direction despite a large demagnetizing field in the width direction.

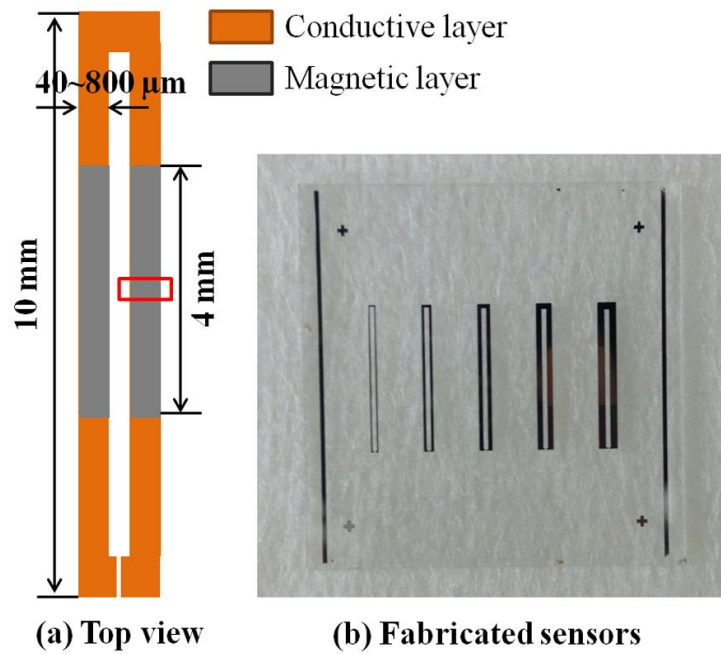


Figure 4.10 (a) Schematic of the sensor structure. The red box denotes the point of the domain observation. The width of the sensor changed from 40 μm to 800 μm . The thickness of the magnetic layer was varied at 0 μm , 1.4 μm , and 2.1 μm . (b) Fabricated sensors (100 μm –500 μm)

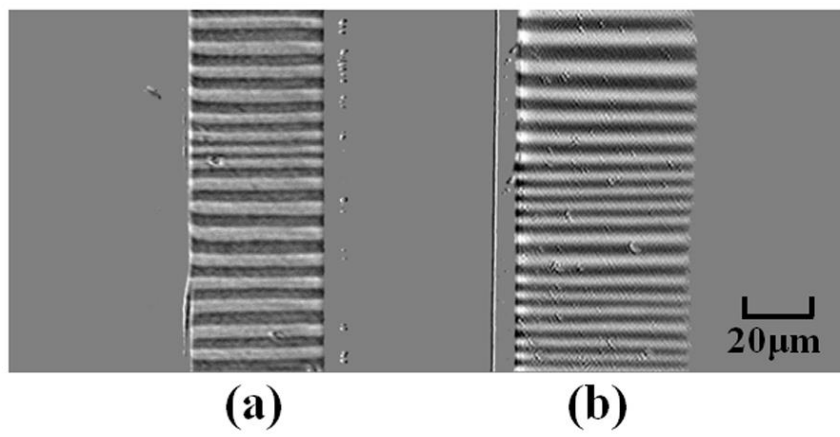


Figure 4.11 Results of the magnetic domain observation with narrow width sensor at (a) 40 μm and (b) 50 μm

Then, the shape anisotropy, induced anisotropy and total induced anisotropy field (H_k) was obtained by calculation and VSM measurement according to changes in the width. The width was increased from 100 μm to 800 μm .

The demagnetizing field was determined by the ratios of the axes lengths. Using the method which was proposed by J. A. Osborn in 1945 [10], I calculated the demagnetizing field of each sensor of a different width. The calculated demagnetizing fields are shown in Fig. 4.12. The demagnetizing field of the width significantly decreased with increases in width, whereas the demagnetizing field of the longitudinal direction was not influenced.

Using these fabricated elements, the magnetic properties were evaluated. Figure 4.13 is the results of VSM measurement. As shown in these magnetization curves, when I applied an external magnetic field in the longitudinal direction, all of the elements were saturated with relatively smaller external magnetic fields, even though the magnetic anisotropy was induced in the transverse direction. However, there were two anisotropies, which were mixed in the magnetization curve: shape anisotropy and induced anisotropy. After subtracting the demagnetizing field by shape anisotropy from the measurement result of the VSM, I could observe only the induced anisotropy part of the magnetic field. Table 4.1 shows the result of dividing the elements into those with shape anisotropy and induced anisotropy. In this table, plus (+) denotes that the transverse direction is the easy axis, and minus (-) denotes that the longitudinal direction is the easy axis. Transverse magnetic anisotropy was induced like the results of domain observation because the induced anisotropy has a plus (+) sign. When the width of the elements increase, the slope of the magnetization curve was increased. This means that I could induce magnetic anisotropy, which was sensitively rotated with a

weak magnetic field.

I also confirmed this by observing the magnetic domain. As shown in Fig. 4.14, the width of the magnetic domain increased with the width of the sensor. The width of magnetic anisotropy was approximately 3.8 μm for 100 μm sample, and the anisotropy increased to 13 μm for the 800 μm sample. A large-width domain has low energy; therefore, it can be rotated easily by a small external magnetic field. Consequently, smaller anisotropy field can be realized in large width because in the sample which has large width, the generated stress caused by mismatch of thermal expansion coefficient between layers is relatively smaller than narrow element, whereupon it has wide magnetic domain structure in wide width element.

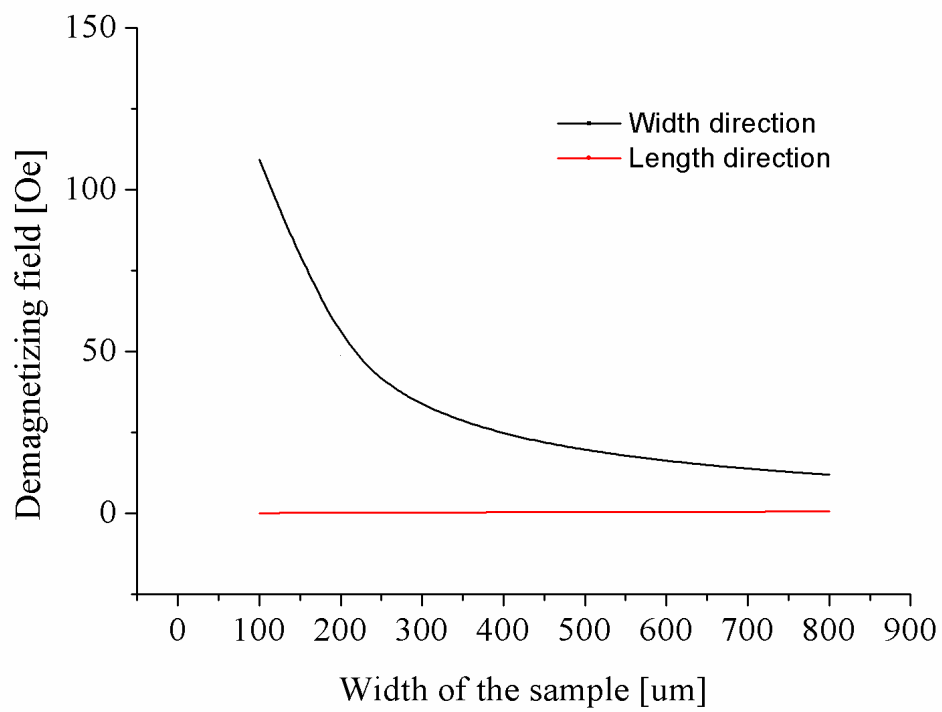


Figure 4.12 Calculation of the demagnetizing field versus the changes in width

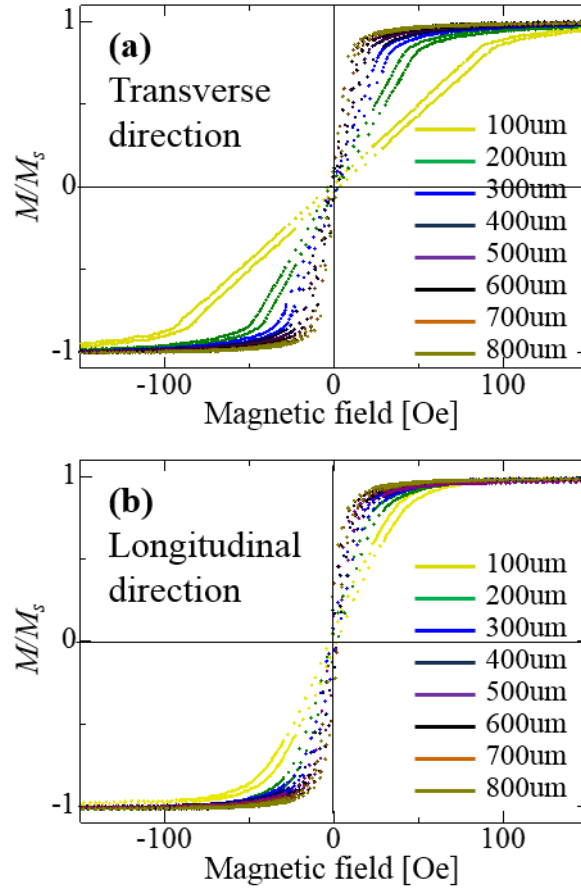


Figure 4.13 Magnetization curves according to changes in the width: (a) Result of the transverse measurement, and (b) result of the longitudinal measurement

TABLE 4.1

Divided into shape anisotropy and induced anisotropy

Width	H_k		
	VSM [Oe]	Shape [Oe]	Induced [Oe]
100 μm	-78	+109	+32
200 μm	-28	+49	+20
300 μm	-16	+32	+16
400 μm	-11	24	+13
500 μm	-6	19	+13
600 μm	-5	16	+10.5
700 μm	-4	13	+9.5
800 μm	-3	12	+8.5

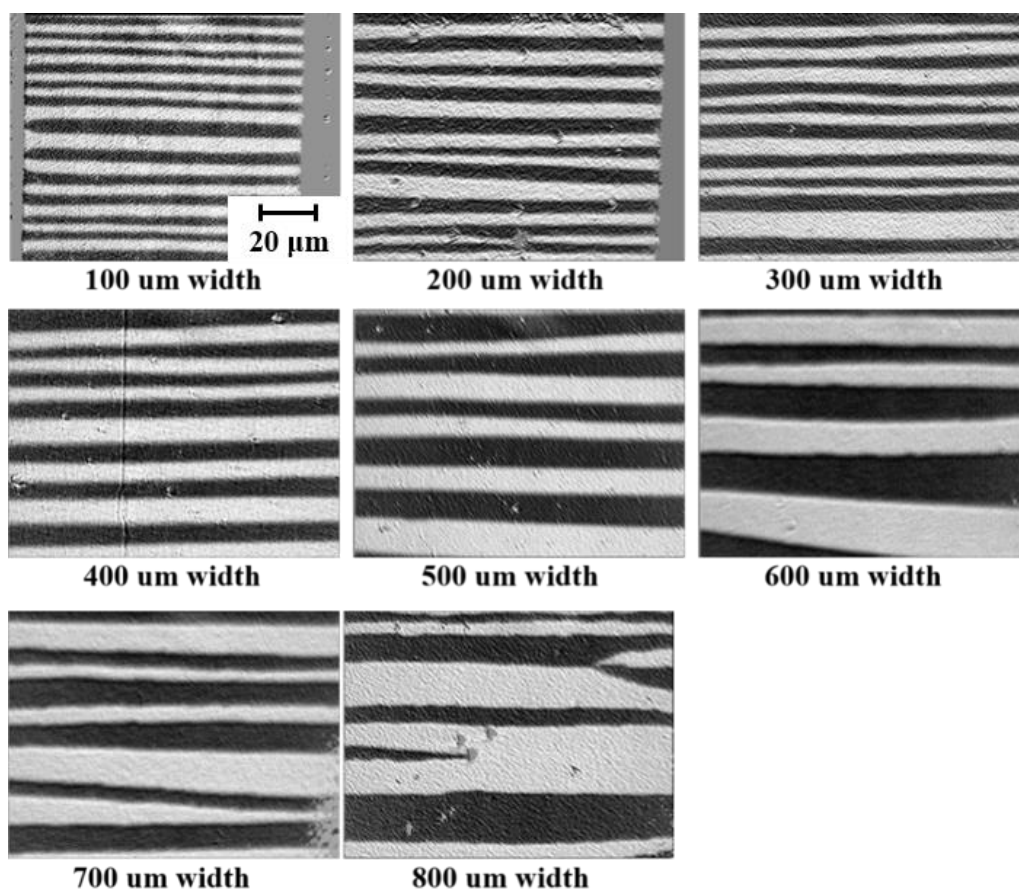


Figure 4.14 Results of magnetic domain observation using Kerr-effect microscopy. The width of magnetic anisotropy increased with the sample width

4.4 Influence of Length of Conductive Layer on Magnetic Anisotropy

The effect of conductive layer's shape on inducing magnetic anisotropy is studied in this chapter.

4.4.1 Fabrication of the elements

$\text{Fe}_{72}\text{Si}_{14}\text{B}_{14}$ and Molybdenum were used for the magnetic and conductive layer, respectively. The thickness of the magnetic layer is $0.7\text{ }\mu\text{m}$ and conductive layer is $2\text{ }\mu\text{m}$. They are insulated by SiO_2 layer of $0.25\text{ }\mu\text{m}$. I fixed the magnetic layers ($1\text{mm} \times 1\text{mm}$) and conductive layer's length is changed from 1 mm to 4 mm , as shown in Fig. 4.15.

4.4.2 Experimental results according to changes in length of the conductive layer

First I carried out observation of magnetic domain structure by Kerr-microscope. The observation results of magnetic domain are as shown in Fig. 4.16. When the magnetic and conductive layer is deposited in equivalent size ($1\text{mm} \times 1\text{mm}$), the uniaxial in-plane magnetic anisotropy was not induced in magnetic layer, because generated stresses are equal to all of direction (Fig. 4.16(a)). In this condition, uniaxial magnetic anisotropy cannot be induced. As the result, magnetic domain pattern randomly appeared as shown Fig. 4.17(a). Expanding the length of conductive layer, the uniaxial magnetic anisotropy was began to induce in magnetic layer because increase of Mo conductive layer's length becomes load and it interrupts the release of stress. Therefore, the difference of stress is occurred in magnetic layer as shown in Fig. 4.16 (b)

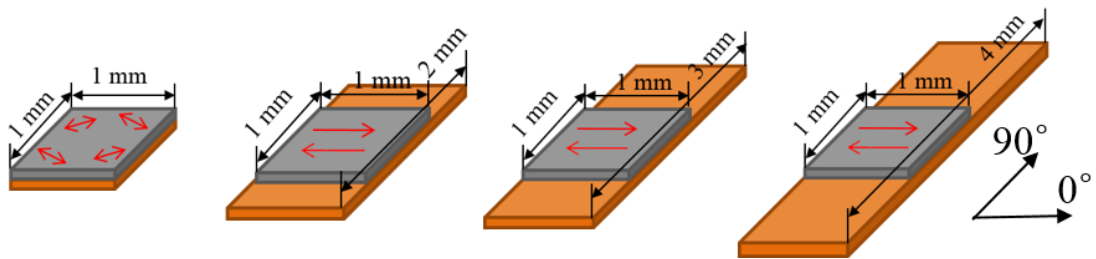


Figure 4.15 A configuration of fabricated thin film according to changes in length of Molybdenum conductive layer. Gray and orange color denotes the magnetic and conductive layer, respectively

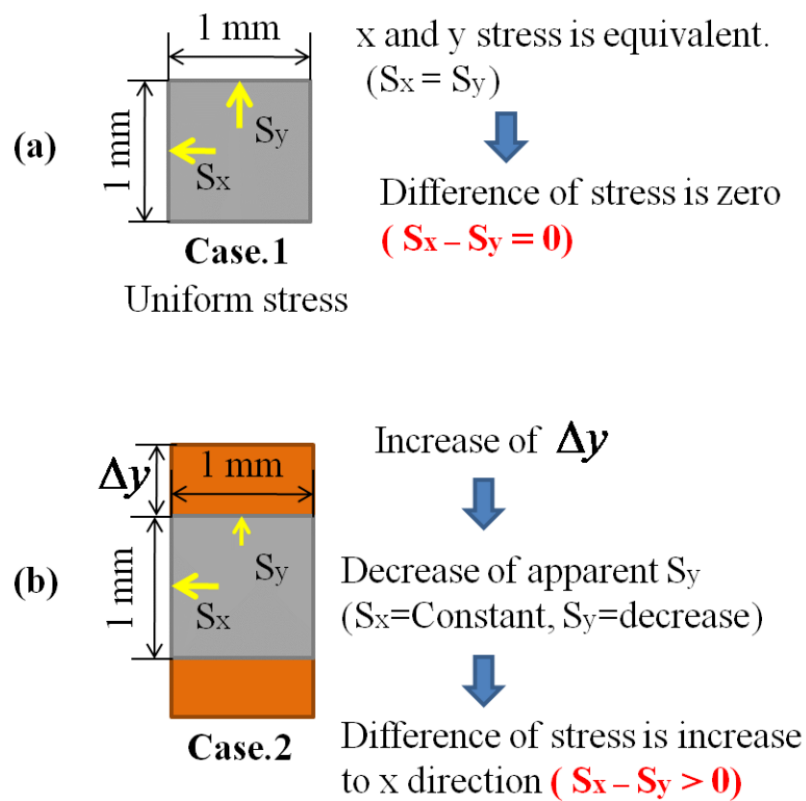


Figure 4.16 A process to change stress difference according to changes in length of conductive layer

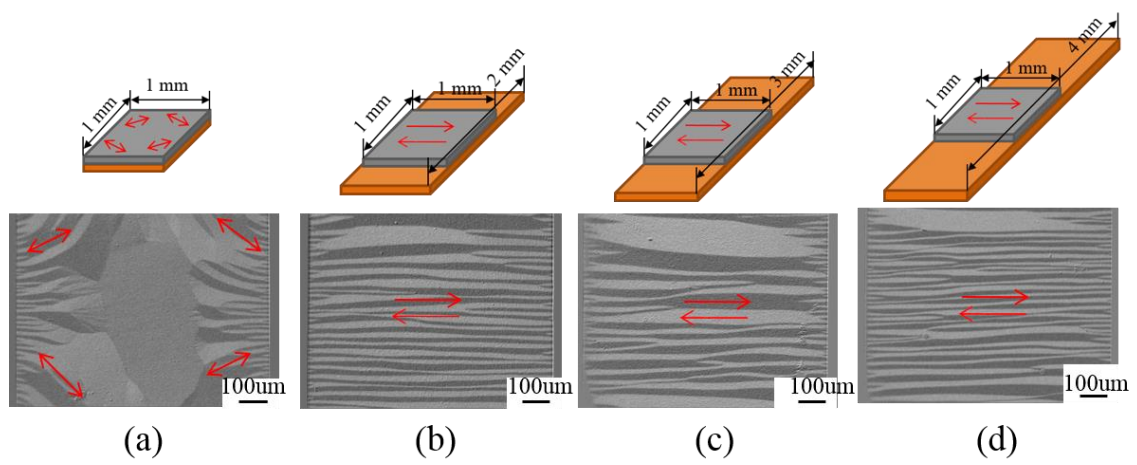


Figure 4.17 A configuration of fabricated thin film according to changes in length of Molybdenum conductive layer. Gray and orange color denotes the magnetic and conductive layer, respectively

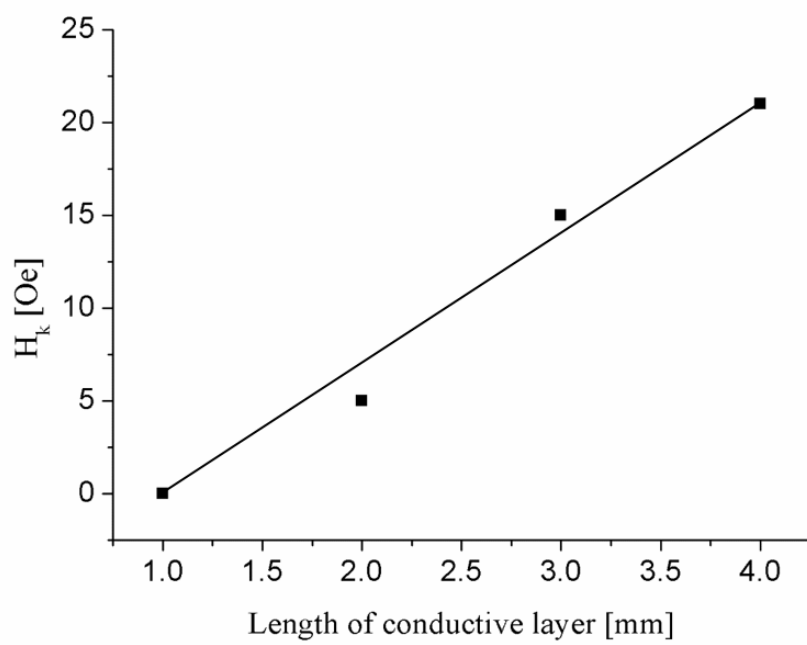


Figure 4.18 A result of H_k measurement according to changes in length of Molybdenum conductive layer

According to increases in length of conductive layer, the uniaxial magnetic anisotropy was induced. It was confirmed by experiment as shown in Fig. 4.17(b) ~ (d). The anisotropy field (H_k) of each samples was measured by VSM. The length of conductive layer can change the induced anisotropy field. The H_k increased with the conductive layer's length from 0 Oe to 22 Oe (see Fig. 4.18).

4.4.3 Experimental results according to changes in shape of the conductive layer

In the chapter of 4.4.2, I investigated the influence of length variation on magnetic anisotropy and its induced anisotropy field. In order to identify a little more about the effects of the conductive layer's shape, I carried out other experiments.

I prepared two divergent type thin film. First, the thin film had isomorphic structure between magnetic and conductive layer as shown in Fig. 4.18(a). The other thin film was prepared as shown in Fig. 4.18(b). In this case, the conductive layer was deposited under the entire area of patterned magnetic layer in the shape of rectangle.

As the results of magnetic domain observation, magnetic anisotropy was induced along the width direction of conductive layer in both cases (see Fig. 4.18((a)1) and Fig. 4.18((b)1)), whereas in the area of 4.18((a)2) and 4.18((b)2), it showed opposite results. However, we could notice that the magnetic anisotropy was induced along the width direction in all the samples. It shows that the direction of induced magnetic anisotropy is dependent on the shape of conductive layer and magnetic anisotropy is transversely induced.

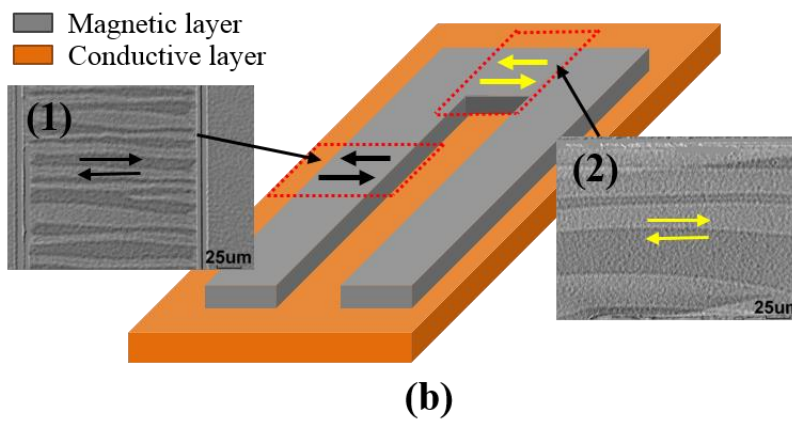
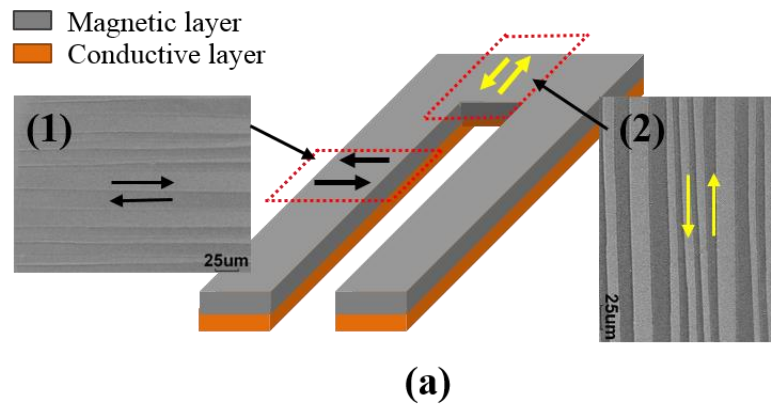


Figure 4.18 A configuration and the results of magnetic domain observation. (a) The shape of magnetic and conductive layer is isomorphic. (b) The conductive layer has rectangular shape under the entire area of patterned magnetic layer

4.5 Summary

This study is required to fabricate high-sensitive MI sensor using the proposed method. As the experimental result, I found that the geometry of sensor elements has influenced magnetic anisotropy and its induced anisotropy field. This results strongly related to generated stresses by changes in geometry.

Based on the experimental results, therefore, when I could establish a design spec for high sensitive MI sensor element. The ratio of the thickness between magnetic and conductive layer should be one to two under the condition which I used FeSiB and molybdenum in magnetic and conductive layer, respectively. The wider width of magnetic layer and small aspect ratio on conductive layer has the advantage of improve the sensitivity. Besides, the direction of induced magnetic anisotropy is dependent on the shape of conductive layer.

References

- [1] B. Hofmann, and H. Kronmuller, "Stress-induced magnetic anisotropy in nanocrystalline FeCuNbSiB alloy," *J. Mag. Mag. Mat.*, **152**, 91-98, 1996.
- [2] H. Q. Guo, H. Kronmuller, T. Dragon, C. Chen, and B. G. Shen, "Transverse domain structure related giant magnetoimpedance in nanocrystalline Fe_{73.5}Cu₁Nb₃Si_{13.5}B₉ ribbons," *J. Appl. Phys.*, **84**, 5673, 1998.
- [3] H. Q. Guo, H. Kronmuller, T. Dragon, Z. H. Gheng, and B. G. Shen, "Influence of nanocrystallization on the evolution of domain patterns and the magnetoimpedance effect in amorphous Fe_{73.5}Cu₁Nb₃Si_{13.5}B₉ ribbons," *J. Appl. Phys.*, **89**, 514, 2001.
- [4] M. Vazquez, G. V. Kuryandskaya, J.M. Garcia-Beneytez, J. P. Sinnecker, J.M. Barandiaran, V. A. Lukshina, and A. P. Potapov, "Frequency dependence of the magnetoimpedance in nanocrystalline FeCuNbSiB with high transverse stress-induced magnetic anisotropy," *IEEE Trans. Magn.*, **35**, 3358-3360, 1999.
- [5] G. V. Kuryandskaya, J.M. Barandiaran, M. Vazquez, D. Garcia, and N.V. Dmitrieva, "Influence of geometrical parameters on the giant magnetoimpedance response in amorphous ribbon," *J. Mag. Mag. Mat.*, **215-216**, 740-742, 2000.
- [6] Raymond A. Serway and John W. Jewett, "*Physics for Scientists and Engineers with Modern Physics*," ISBN-13: 978-0534408442, 2003.
- [7] K. H. Shin, Y. H. Kim, K. I. Park, and G. Sa-Gong, "Anisotropy Control of Highly Magnetostrictive Films by Bias Stress," *JKMS.*, **13**, 193-197, 2003.
- [8] K. Wasa, M. Kitabatake, and H. Adichi, "*Thin Film Materials Technology*," ISBN:

0-8155-1483-2, 2004

- [9] Y. Suwa, S. Agatsuma, S. Hashi, and K. Ishiyama, "Study of Strain Sensor Using FeSiB Magnetostrictive Thin Film," *IEEE Trans. Magn.*, **46**, 666-669, 2010.
- [10] I. Taher, M. Aslam, M. A. Tamor, T. J. Potter, and R. C. Elder, "Piezoresistive microsensors using p-type CVD diamond films," *Sens. Actuators A.*, **45**, 35-43, 1994.
- [11] Forrest G. West, "Uniaxial Anisotropy due to Magnetoelastic Energy in Constrained Polycrystalline Films," *J. Appl. Phys.*, **35**, 1827-1840, 1964.
- [12] S. Timoshenko, "Analysis of bi-metal thermostats," *J. Opt. Soc. Am.* **11**, 233-255, 1925.
- [13] C. Yokota, K. Ishiyama, and K. I. Arai, "Comparison with film substrates of polyimide and Ni for cantilevered magnetic actuators," *IEEJ Trans.*, **2**, 436-439, 2007.
- [14] B. D. Cullity and C. D. Graham, "Introduction to Magnetic Material," ISBN: 987-0-471-47741-9, 2009.
- [15] J. A. Osborn, "Demagnetizing Factors of the General Ellipsoid," *Phys. Rev.* **67**, 351, 1945.

Chapter 5

Investigation of Magnetic Properties According to Changes in Magnetic Material

5.1 Introduction

The sensitivity of MI sensor element strongly relates to induced magnetic anisotropy and variation of the permeability [1]-[3]. Therefore, it is very important to produce the magnetic anisotropy which rapidly reacts and change the direction by small external magnetic field [4]-[8]. As I mentioned above, impedance is the minimum with transverse magnetic anisotropy. According to applying external magnetic field, the impedance increases and the maximum impedance value appears when the external magnetic field becomes equal in anisotropy field (H_k) of the elements [9], [10]. Hence, H_k has to be as small as possible. For reduction of H_k value, I controlled the generated stress according to varies in the geometry of element in chapter 4 [11], [12]. However, it

is not enough to reduce H_k for high sensitivity of MI sensor element. Besides, there is a limitation to control geometry of the thin film. As the reason, much more need of consideration to change magnetostriction constant because the generated magnetoelastic energy has relations not only stresses (σ) but also the magnetostriction constant (λ_s) as follow [13], [14]:

$$E_{me} = \frac{3}{2} \lambda_s \sigma = \frac{1}{2} H_k M_s \quad (5.1)$$

where E_{me} is induced magnetoelastic energy in the magnetic layer. H_k is anisotropy field, M_s is the saturation magnetization. λ_s is the saturation magnetostriction, and σ is the stress in the thin film.

In this chapter, I addressed the influence of the magnetostriction constant on the magnetic anisotropy and the sensitivity with which the anisotropy can be controlled.

For the investigation of the effect of the magnetostriction constant, I used two materials: FeSiB and CoFeSiB in magnetic layer. The magnetostriction constant decreases according to increase cobalt content. I observed how changes in the ratio of cobalt to iron affected the induction and magnetization of the magnetic anisotropy using impedance measurements and observations of the magnetic domain and magnetization curve.

5.2 Variation of Composition in CoFeSiB

I prepared thin film type elements. The element has double layer: magnetic and conductive layer. The conductive and magnetic layers were 1.8 μm and 0.7 μm thick, respectively. These two layers were insulated with a SiO_2 layer. Fig. 5.1(a) shows the configuration of the fabricated element. It was 100 μm wide and has a one turn conductive layer. The conductive layer of molybdenum was deposited onto a slide glass substrate 1 mm in thickness. Magnetic layers consisting of CoFeSiB or FeSiB were deposited on the conductive layer by radio frequency magnetron sputtering. The sputtering conditions of each layer are shown in TABLE 5.1.

I deposited the CoFeSiB magnetic layer using a $\text{Co}_{70}\text{Si}_{17}\text{B}_{13}$ target with changes in number of Fe chips as shown in Fig. 5.2. The Fe chip were prepared 2 different size (10×10mm and 5×5mm). After deposition, the composition of the CoFeSiB was investigated by scanning electron microscopy-energy-dispersive X-ray spectroscopy. The results is as shown in TABLE 5.2. The magnetostriction constant was obtained by previous study [15]. As the results, magnetostriction constant decreased with addition of iron. FeSiB has 30×10^{-6} magnetostriction constant. When I deposited CoFeSiB using CoSiB target with two Fe chip (10×10 mm), magnetostriction constant decreased one tenth (3×10^{-6}). There was no iron in the magnetic layer (CoSiB), the magnetostriction constant became negative (-4×10^{-6}).

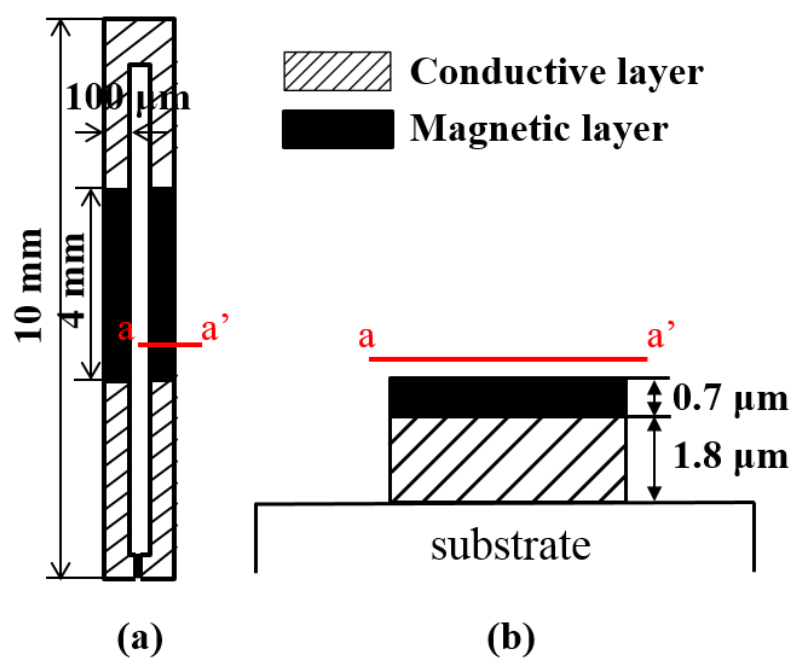


Figure 5.1 Configuration of fabricated element. (a) Top view (b) Cross section view from a to a'

TABLE 5.1
Sputtering condition

	Material			
	Molybdenum	SiO ₂	CoFeSiB	FeSiB
Ar Gas [mTorr]	12	4	18	16
Power [W]	100	100	150	100

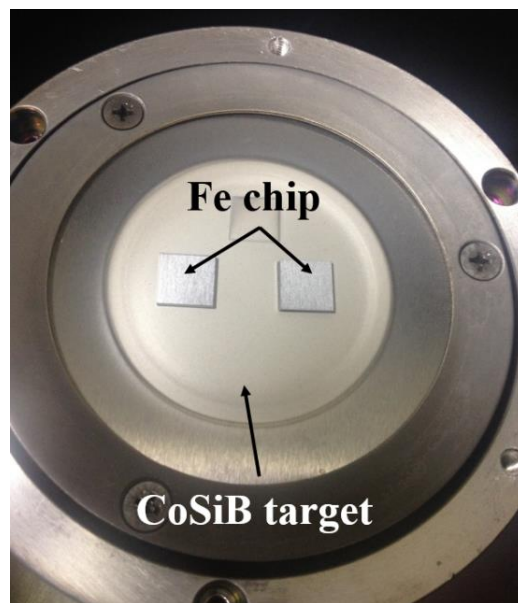


Figure 5.2 A method of CoFeSiB composition. Using $\text{Co}_{70}\text{Si}_{17}\text{B}_{13}$ with pure Fe chips, the magnetostriction constant is controlled

TABLE 5.2
Composition rate and its magnetostriction constant

	Magnetostriction constant	Ratio between Co and Fe by EDX
FeSiB	30×10^{-6}	0 : 100
CoFeSiB (Fe chip 4ea 10x10)	Unknown	77 : 23
CoFeSiB (Fe chip 3ea 10x10, 1ea 5x5)	Unknown	81 : 19
CoFeSiB (Fe chip 3ea 10x10)	Unknown	83 : 17
CoFeSiB (Fe chip 2ea 10x10, 1ea 5x5)	Unknown	86 : 14
CoFeSiB (Fe chip 2ea 10x10)	3×10^{-6}	88 : 12
CoFeSiB (Fe chip 1ea 10x10, 1ea 5x5)	1.5×10^{-6}	91 : 9
CoFeSiB (Fe chip 1ea 10x10)	0×10^{-6}	93 : 7
CoSiB	-4×10^{-6}	100 : 0

5.3 Magnetic Properties of CoFeSiB Samples by Changes in Magnetostriction Constant

I compared two samples, FeSiB ($\lambda_s: 30 \times 10^{-6}$) and CoFeSiB ($\lambda_s: 3 \times 10^{-6}$) to investigate the effect of the magnetostriction constant on the magnetic anisotropy. Fig. 5.3 shows the results of the magnetic domain observation. The observations were conducted in the central area of the magnetic layer because the magnetic domain structures were uniform throughout this area. In the FeSiB layer [Fig. 5.3(a)], domains were uniformly induced along the transverse direction of the layer and it had only a small closure domain. The domain pattern was approximately 3.4 μm and 6.6 μm wide in the FeSiB and CoFeSiB layers, respectively. In comparison with the FeSiB layer, the width of the domain pattern in the CoFeSiB doubled with decreases in the magnetostriction constant. These domain patterns showed that the generated energy of strain induced magnetic anisotropy in the magnetic layer decreased as the magnetostriction constant was reduced. Using these fabricated samples, I confirmed the variations in the domain patterns by applying a magnetic field along the longitudinal direction of element. Fig. 5.4 shows the results of the domain observation under the external magnetic field. When FeSiB was used for the magnetic layer [Fig. 5.4(a)], the direction of magnetic anisotropy was gradually changed from the transverse to the longitudinal direction by the external magnetic field. It was completely saturated at 80 Oe. On the other hand, in the CoFeSiB layer [Fig. 5.4(b)], the induced magnetic anisotropy was easily magnetized by relatively weak magnetic fields. In this case, it was saturated at 10 Oe.

I then evaluated the hysteresis loops of the fabricated elements using a VSM (Fig. 5.4). The magnetic properties were measured in the longitudinal [Fig. 5.5(a)] and

transverse direction [Fig. 5.5(b)]. The hysteresis loops for the transverse direction had a more gradual slope than those for the longitudinal direction because of the large demagnetizing field due to the shape anisotropy. The coercivity of both elements was approximately 1.5 Oe. The sample using CoFeSiB for the magnetic layer reached saturation more rapidly than the one using FeSiB. The FeSiB and CoFeSiB layers were saturated at 80 Oe and 10 Oe, respectively. The trend of magnetization process corresponds to the changes of the domain pattern.

These features indicate that higher sensitivity can be obtained by decreasing the magnetostriction constant. However, if the magnetostriction constant is nearly zero or negative, magnetic anisotropy cannot be induced in the transverse direction. It was verified experimentally as shown in Fig. 5.6.

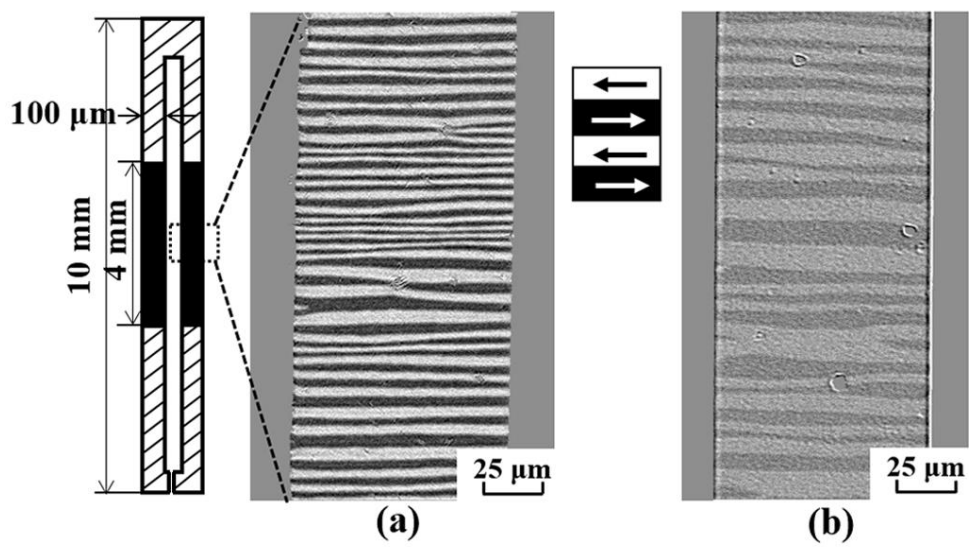


Figure 5.3 Results of magnetic domain observation of the central area of the magnetic layer. (a) FeSiB magnetic layer. (b) CoFeSiB magnetic layer

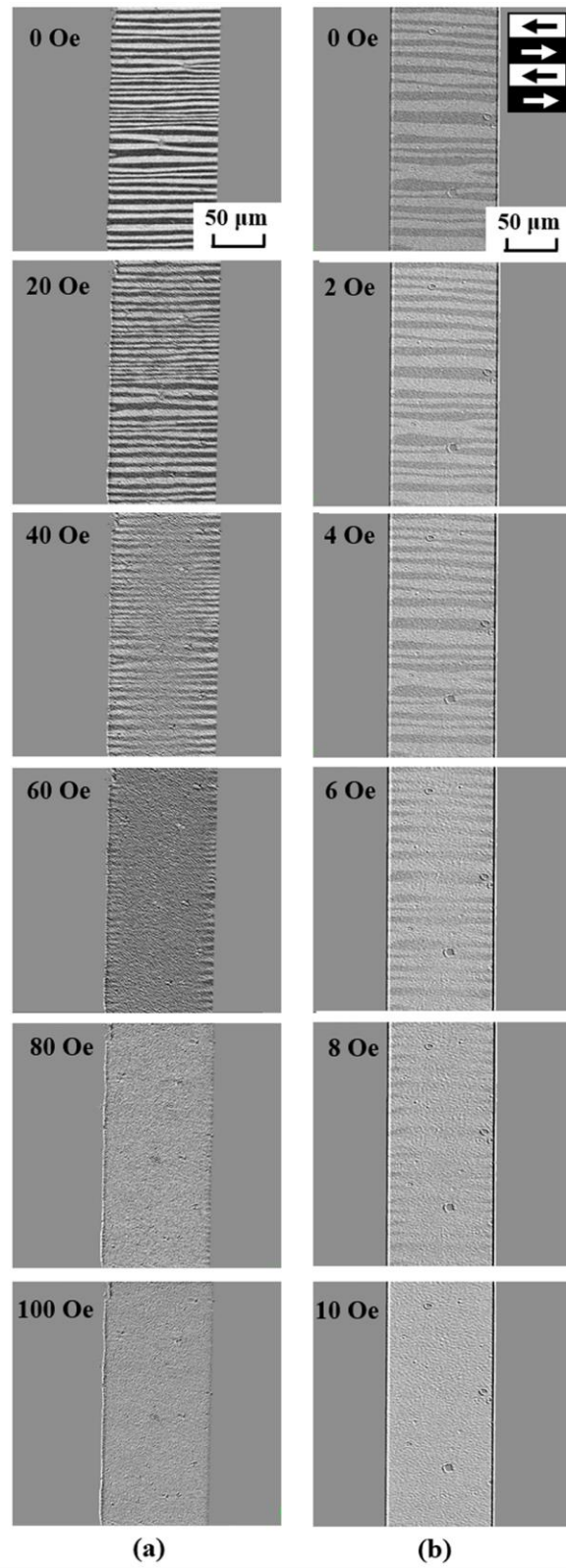


Figure 5.4 Domain patterns observed during magnetization along the longitudinal direction using Kerr-effect microscopy. (a) FeSiB layer (b) CoFeSiB layer

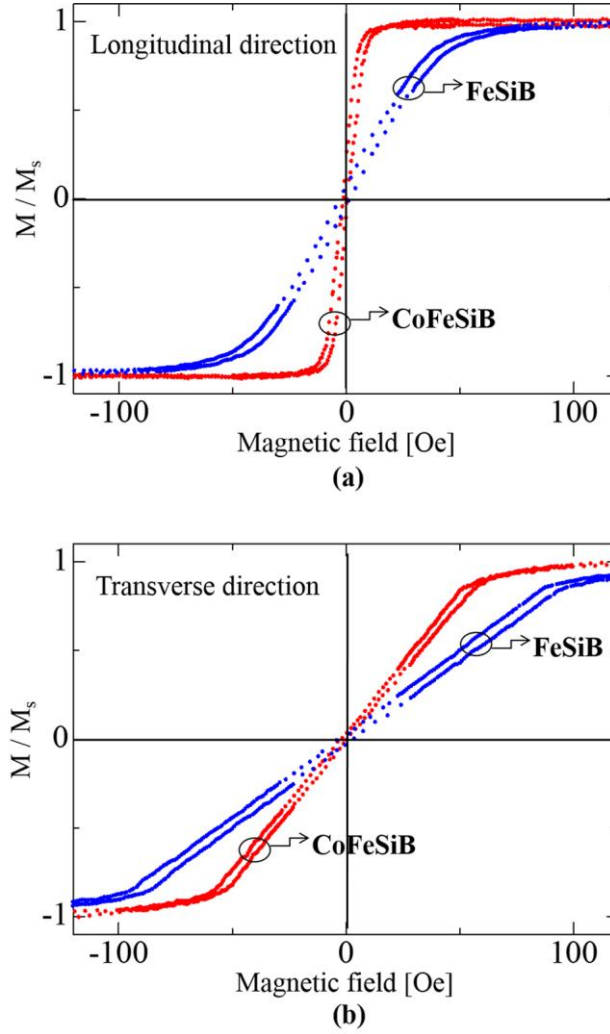


Figure 5.5 Magnetization curves according to changes in magnetostriction constant. Hysteresis loops with external magnetic field applied along the (a) longitudinal and (b) transverse directions of the element

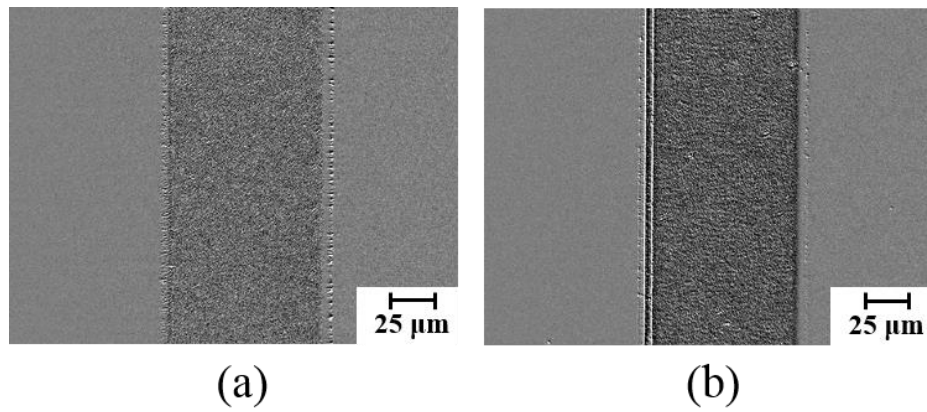


Figure 5.6 Magnetic domain observation for detection of transverse magnetic anisotropy.

(a) Magnetostriction constant is nearly zero (0×10^{-6}) (b) Magnetostriction constant is negative (-4×10^{-6})

5.4 Summary

This study attempted to establish the relationship between the magnetostriction constant and the induction of magnetic anisotropy. I confirmed a strong relationship between the magnetostriction constant and magnetic anisotropy. As the magnetostriction constant decreased, the energy of strain induced magnetic anisotropy generated in the magnetic thin film was reduced. Consequently, using a relatively low magnetostriction constant of magnetic film can induce magnetic anisotropy that rotates direction easily under a weak magnetic field. The FeSiB and CoFeSiB layers were saturated at 80 Oe and 10 Oe, respectively. Thus, a lower magnetostriction constant in the magnetic layer caused a quick response of the impedance variation with improved sensitivity.

This study is important for the development of thin film MI sensors using a stress induction method.

References

- [1] L. Panina and K. Mohri, "Magneto-impedance effect in amorphous wires," *Appl. Phys. Lett.*, **65**, 1189-1191, 1994.
- [2] T. Nakai, H. Abe, S. Yabukami, and K. I. Arai, "Impedance property of thin film GMI sensor with controlled inclined angle of stripe magnetic domain," *J. Mag. Mag. Mat.*, **290-291**, 1355-1358, 2005.
- [3] M. Takezawa, H. Nakagawa, H. Kikuchi, S. Agatsuma, K. Ishiyama, M. Yamaguchi, and K. I. Arai, "Possibility of Sensitive Magnetic Thin-Film Sensor Using LC Resonance," *J. Magn. Soc. Jpn.*, **21**, 661-664, 1997.
- [4] R. L. Sommer and C. L. Chien, "Role of magnetic anisotropy in the magnetoimpedance effect in amorphous alloys," *Appl. Phys. Lett.*, **67**, 857-859, 1995.
- [5] K. Mohri, L. V. Panina, T. Uchiyama, K. Buchida and M. Noda, "Sensitive and Quick Response Micro Magnetic Sensor Utilizing Magneto-Impedance in Co-rich Amorphous Wires," *IEEE Trans. Magn.*, **31**, 1266-1275, 1995.
- [6] L. Kraus, "Theory of giant magneto-impedance in the planar conductor with uniaxial magnetic anisotropy," *J. Mag. Mag. Mat.*, **195**, 764-778, 1999.
- [7] N. A. Usov, A. S. Antonov, and A. N. Lagar'kov, "Theory of giant magneto-impedance effect in amorphous wires with different types of magnetic anisotropy," *J. Mag. Mag. Mat.*, **185**, 159-173, 1998.
- [8] A. Saad, J. A. Garcia, G. Kurlyandskaya, J. D. Santos, and L. Elbaile, "Influence of Residual Stresses and Their Relaxation on Giant Magnetoimpedance of

CoFeSiB Metallic Glasses,” *Jpn. J. Appl. Phys.*, **44**, 4939-4944, 2005

- [9] R. L. Sommer and C. L. Chien, “Longitudinal and transverse magnetoimpedance in amorphous Fe_{73.5}Cu₁Nb₃Si_{13.5}B₉ films,” *Appl. Phys. Lett.*, **67**, 3346-3348, 1995.
- [10] D. Atkinson and P. T. Squire, “Experimental and Phenomenological Investigation of the Effect of Stress on Magneto-Impedance in Amorphous Alloys,” *IEEE Trans. Magn.*, **33**, 3364-3366, 1997.
- [11] J. W. Shin, S. H. Kim, S. Hashi, and K. Ishiyama, “The Dependence of Magnetic Anisotropy on the Ratio of Thickness,” *JKPS.*, **63**, 616-680, 2013.
- [12] J. W. Shin, Y. Miwa, S. H. Kim, S. Hashi, and K. Ishiyama, “Observation of the magnetic properties according to changes in the shape of thin-film giant magnetoimpedance sensor,” *IEEE Trans. Magn.*, to be published.
- [13] I. Taher, M. Aslam, M. A. Tamor, T. J. Potter, and R. C. Elder, “Piezoresistive microsensors using p-type CVD diamond films,” *Sens. Actuators A.*, **45**, 35-43, 1994.
- [14] Forrest G. West, “Uniaxial Anisotropy due to Magnetoelastic Energy in Constrained Polycrystalline Films,” *J. Appl. Phys.*, **35**, 1827-1840, 1964.
- [15] V. Madurga, M. Vazquez, A. Hernando, and O. V. Nielsen, “Magnetostriction of amorphous (Co_{1-x}Fe_x)₇₅Si₁₅B₁₀ ribbons (0<x<0.12) and its temperature dependence,” *Solid State Comm.*, **52**, 701-703, 1984.

Chapter 6

Sensor Application

6.1 Introduction

This research focused on inducing and controlling magnetic anisotropy utilizing the proposed method which I suggested [1]. It was studied for development of MI sensor element. So far, many of MI sensors have proposed for various method and purpose, such as magnetic recording devices [2], bio-signal sensing [3], [4], etc. It is widely recognized that the MI sensor can detect magnetic field according to changes in impedance value [5]-[12]. The rate of impedance variation can be achieved as follow [13], [14]:

$$\text{Rate of impedance variation (\%)} = \frac{Z_m - Z_0}{Z_0} \times 100 \quad (6.1)$$

where Z_m and Z_0 are maximum impedance with field and initial impedance without

field values, respectively.

As Therefore, based on previous research result, I fabricated prototype MI sensor element according to changes in geometries and magnetic materials. I measured impedance variation when the element was subjected to an alternating current with applying a magnetic field.

Figure 6.1(a) shows a measurement system of the impedance. The element was set into a pair of Helmholtz coil and AC current flowed perpendicular to transverse magnetic anisotropy by a sourcemeter. The DC external magnetic field is parallel with AC current. According to the applied magnetic field along the longitudinal direction, the impedance increased until the transverse magnetic anisotropy became parallel with external magnetic field. It was measured by Network Analyzer. The sensor element was contact with a probe as shown in Fig. 6.1(b).

6.2 Experimental Analysis

6.2.1 Impedance measurement according to changes in length of conductive layer

I fabricated a prototype comprising multi-layered structure thin-film MI sensor element according to changes in the length of conductive layer.

I expected that the rate of impedance variation improve according to the decrease of the conductive layer's length because the minimum induced anisotropy field (H_k) was obtained in very short conductive layer as shown in Fig. 6.2. It was confirmed by experiments in chapter 4.4.

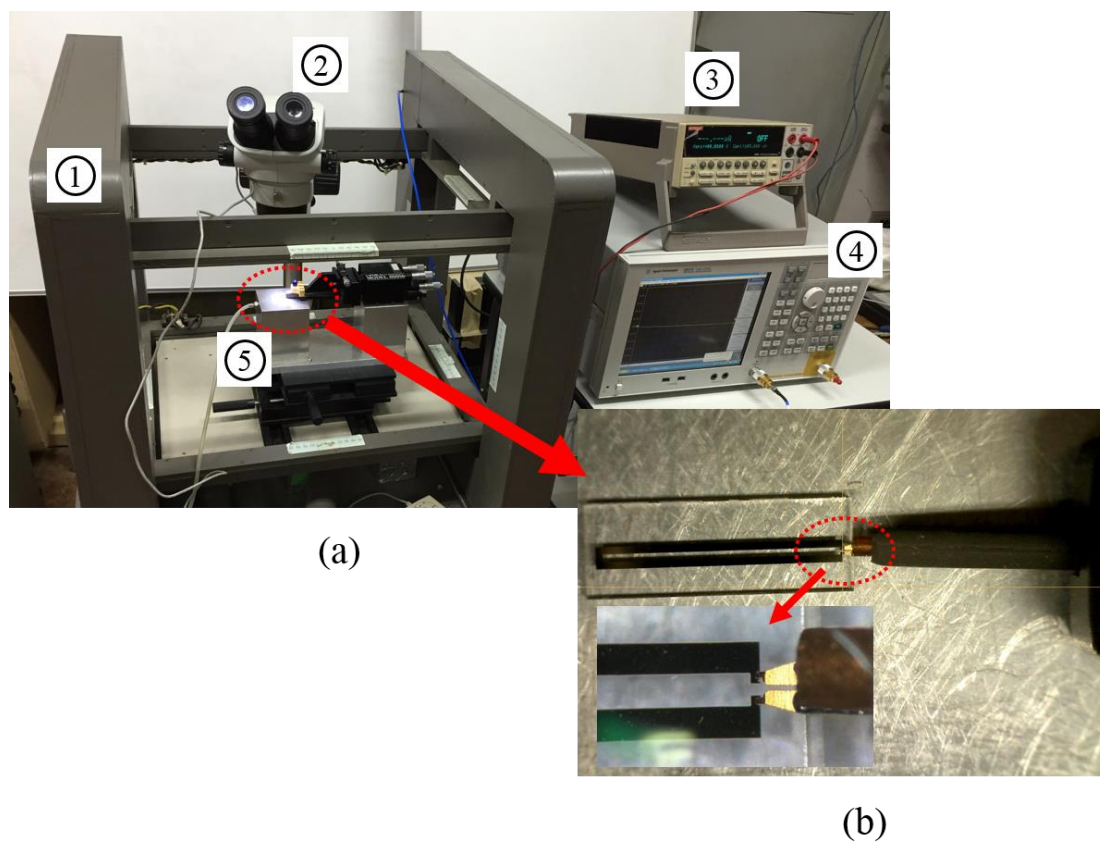
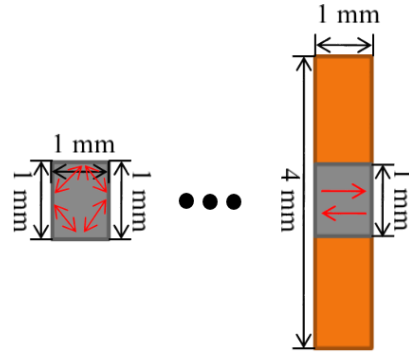
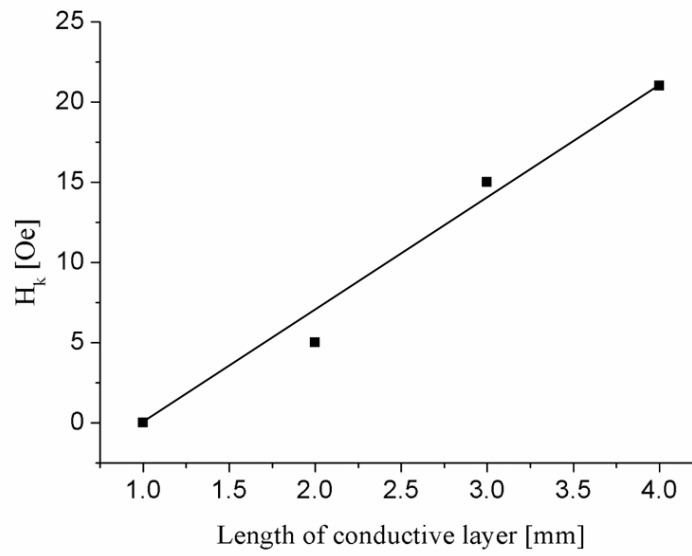


Figure 6.1 (a) Configuration of impedance measurement system: ① Helmholtz coil, ② Microscope, ③ Soucemeter, ④ Network analyzer, ⑤ Sample stage. (b) Probe for measurement and picture of the mounted element



(a)



(b)

Figure 6.2 (a) Configuration of fabricated thin film according to changes in the length of conductive layer (b) Measured anisotropy field (H_k)

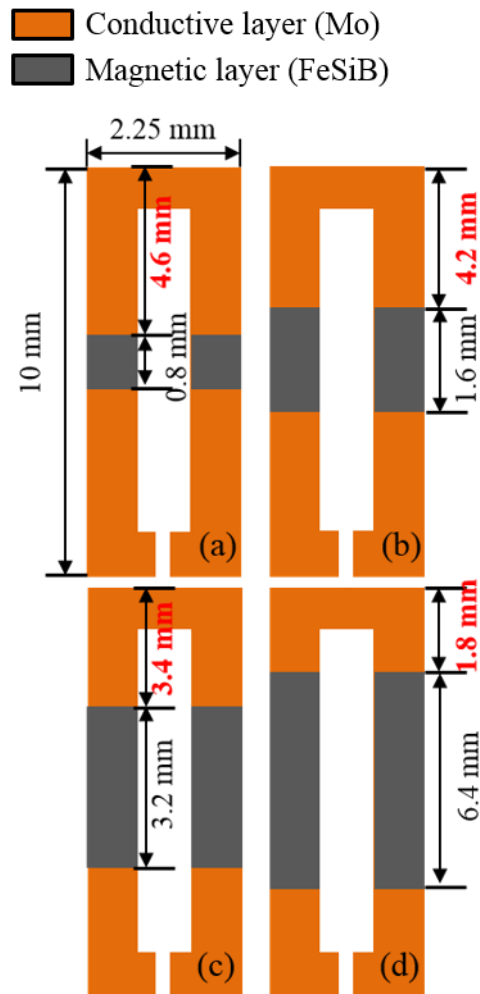


Figure 6.3 Configuration of the fabricated MI sensor elements (a) Length of conductive layer is 4.6 mm (b) 4.2 mm (c) 3.4 mm (d) 1.8 mm

Figure 6.3 shows the fabricated sensor elements. The samples were prepared four types with decreases in the length of conductive layer from 4.6 mm [Fig. 6.3(a)] to 1.8 mm [Fig. 6.3(d)]. I fixed the magnetic layers (1mm × 1mm). $\text{Fe}_{72}\text{Si}_{14}\text{B}_{14}$ and Molybdenum were used for the magnetic and conductive layer, respectively. The thickness of the magnetic layer is 0.7 μm and conductive layer is 2 μm . They are insulated by SiO_2 layer of 0.25 μm . Magnetization curves of the different lengths of the conductive layer elements were measured in a transverse and longitudinal direction. As shown in Fig. 6.4, decreases in the length caused quick saturated magnetization when the magnetic field was applied along the longitudinal direction of the sensor. The sensor response to the magnetic field became faster in comparison with the starting point of impedance increase at each element. For example, in case of a 4.6 mm length element, the point of saturation of magnetization appeared over 40 Oe, approximately, whereas in case of the 1.8 mm element, the magnetization of saturation reached rapidly at a magnetic field of 5 Oe, approximately.

Using these samples, I carried out impedance measurement. The results is as shown in Fig. 6.5. The impedance rapidly reached to maximum impedance at lower DC field by decreasing of the conductive layer's length. Hence, the rate of impedance variation increased from 0.004 Ω/Oe to 0.164 Ω/Oe at the length of 4.6 mm to 1.8 mm. It presents that the impedance changes fast in a small magnetic field. Moreover, the impedance change amounts also were increased in proportion to the growth of volume of the magnetic layer.

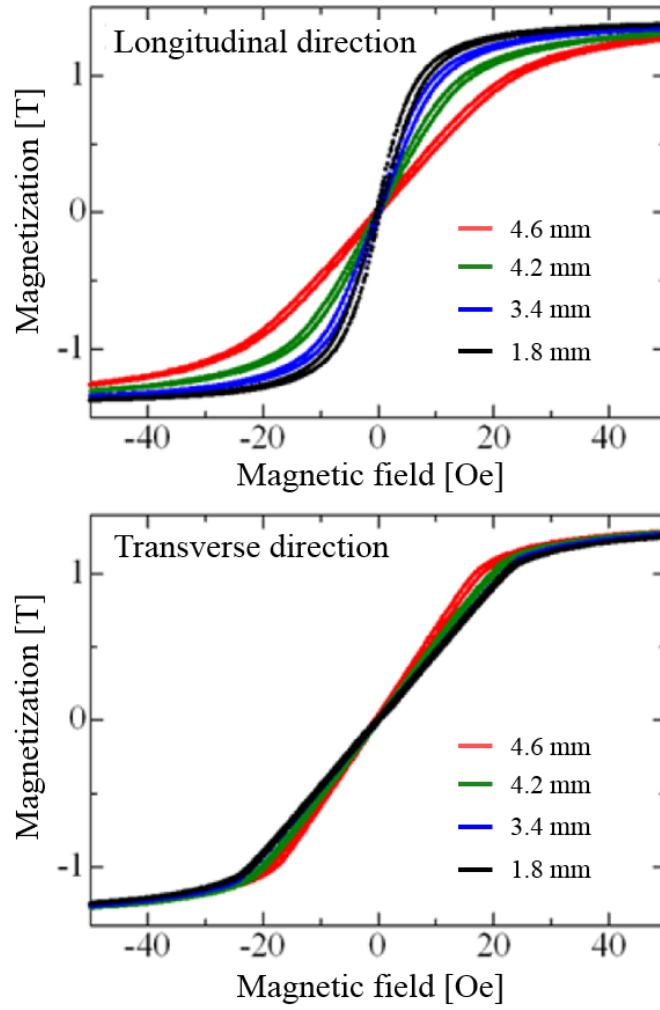


Figure 6.4 Hysteresis loops measuring transverse and longitudinal direction according to changes in length of the conductive layer

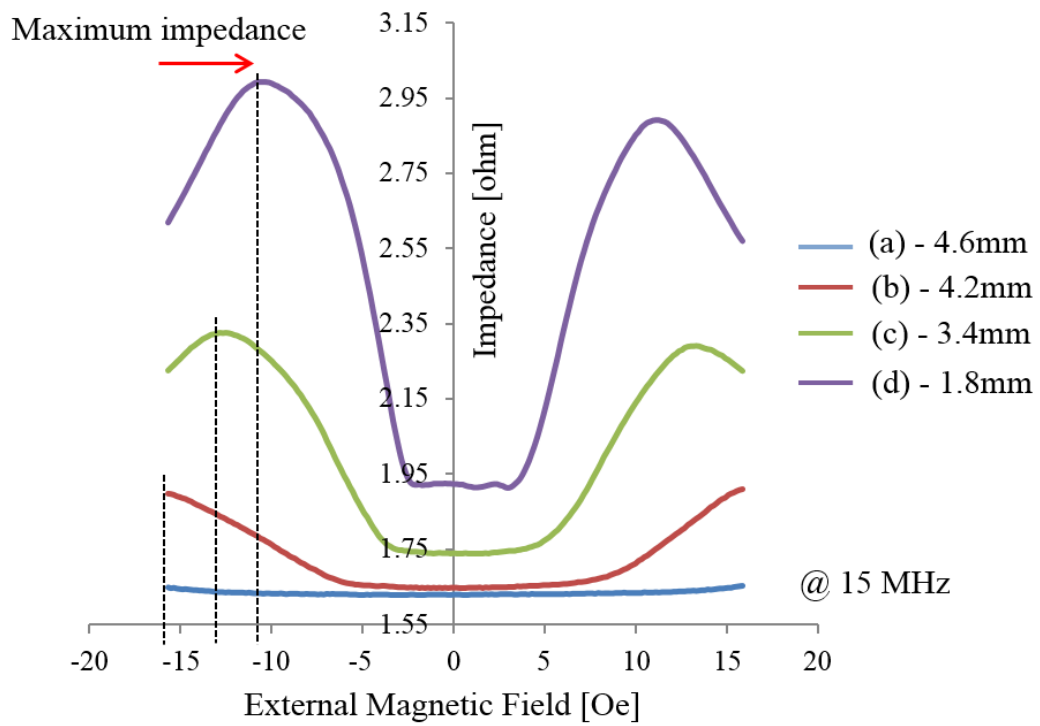


Figure 6.5 The results of impedance measurement with changes in the length of conductive layer from 4.6 mm to 1.8 mm

6.2.2 Impedance measurement according to changes in magnetostriction constant

For investigation of magnetostriction constant effect, I prepared two types of elements. The element has double layer: magnetic and conductive layer. The conductive and magnetic layers were 1.8 μm and 0.7 μm thick, respectively. The sample has 100 μm wide and a one turn conductive layer [see Fig. 6.6(a)]. These two layers were insulated with a SiO_2 layer. The conductive layer of molybdenum was deposited onto a slide glass substrate 1 mm in thickness. Magnetic layers consisting of CoFeSiB or FeSiB were deposited on the conductive layer by radio frequency magnetron sputtering. I deposited the CoFeSiB magnetic layer using a $\text{Co}_{70}\text{Si}_{17}\text{B}_{13}$ target with two Fe chips (10 mm \times 10 mm). After deposition, the composition of the CoFeSiB was investigated by scanning electron microscopy-energy-dispersive X-ray spectroscopy. The results indicated that the ratio of cobalt to iron was approximately 88 at.% to 12 at.%. As this ratio, the magnetostriction constant of CoFeSiB was estimated to 3×10^{-6} [9]. I then measured the impedance variation. An AC current flowed through the conductive layer and the DC external magnetic field was applied along the longitudinal direction of element. Under the applied magnetic field (from -16 Oe to +16 Oe) along the longitudinal direction, the impedance increased until the transverse magnetic anisotropy became parallel to the external magnetic field. For the CoFeSiB layer [Fig. 6.6(c)], the maximum impedance appeared at an applied field of approximately 8 Oe. Fig. 5(c) shows the results for the FeSiB layer. Unlike the results for CoFeSiB, the impedance changed gradually in the FeSiB layer. Strong magnetic anisotropy was induced because of the higher magnetostriction constant. When the magnetic sensor element was fabricated using CoFeSiB with molybdenum conductive layer, it showed 14% (2.5%/Oe) impedance variation rate.

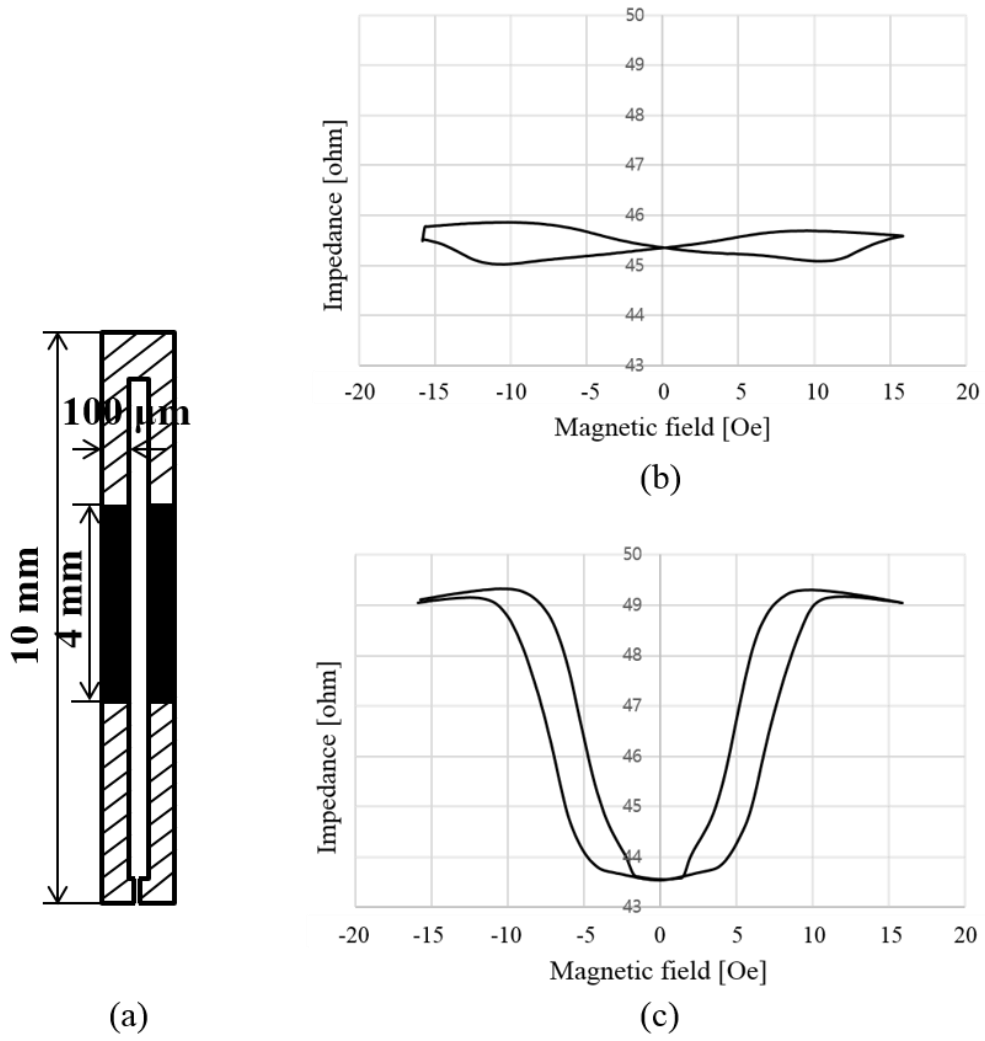


Figure 6.6 (a) A Configuration of fabricated element and Results of impedance measurement at 100 MHz. The external magnetic field was applied from -16 Oe to +16 Oe. (a) FeSiB layer (b) CoFeSiB layer

Unfortunately, I could not obtain an accurate result of FeSiB sample because output of magnetic field of our measurement setup was limited to ± 16 Oe. As the results, using the magnetic material which has a relatively lower magnetostriction constant can improve the rate of impedance variation.

6.3 Comparison with Current Magnetic Sensors

In this chapter, I will evaluate rate of impedance variation of the sensor element, which I fabricated, with other current MI sensor elements. In addition, the characteristic of my sensor element will be compared with other type magnetic sensors.

There are many research about MI sensor element with the thin film and these elements showed 8%/Oe at 80 MHz [15], 5%/Oe [16], 40%/Oe [17] and %/Oe [8] impedance variation. In comparison with those elements, the MI sensor element, which I fabricated, has 2.5%/Oe rate of impedance variation, as shown in Table 6.1. Although achieved impedance variation of the sensor element, which was fabricated by my proposed method, was almost same or rather less. However, this impedance variation result was obtained by relatively simpler method. Therefore, I tentatively consider that the sensitive sensor element can be realized by the proposed method. In addition, it has advantages in mass production and cost cutting due to simple fabrication process.

From the previous research [16], the fabricated element using the proposed method will have approximately 10^{-6} Oe resolution. This sensitivity can be located in the middle of detection range of general MI sensor, as shown in fig. 6.7. This sensitivity is not enough to use for bio signal detection, however it can be used general applications such as navigation, position and earth magnetic field detection. Besides, the fabricated sensor

TABLE 6.1
Comparison of thin film type MI sensor elements

Magnetic material	Rete of impedance variation	Method for inducing magnetic anisotropy	Reference
CoFeB	8%/Oe	Annealing in magnetic field	[15]
NeFe	5%/Oe	Deposition in magnetic field	[16]
NiFe	40%/Oe	Annealing in magnetic field	[17]
CoNbZr	50%/Oe	Annealing in magnetic field	[8]
CoFeSiB	2.5%/Oe	Inverse-magnetostrictive effect with residual stress by thermal expansion coefficient	

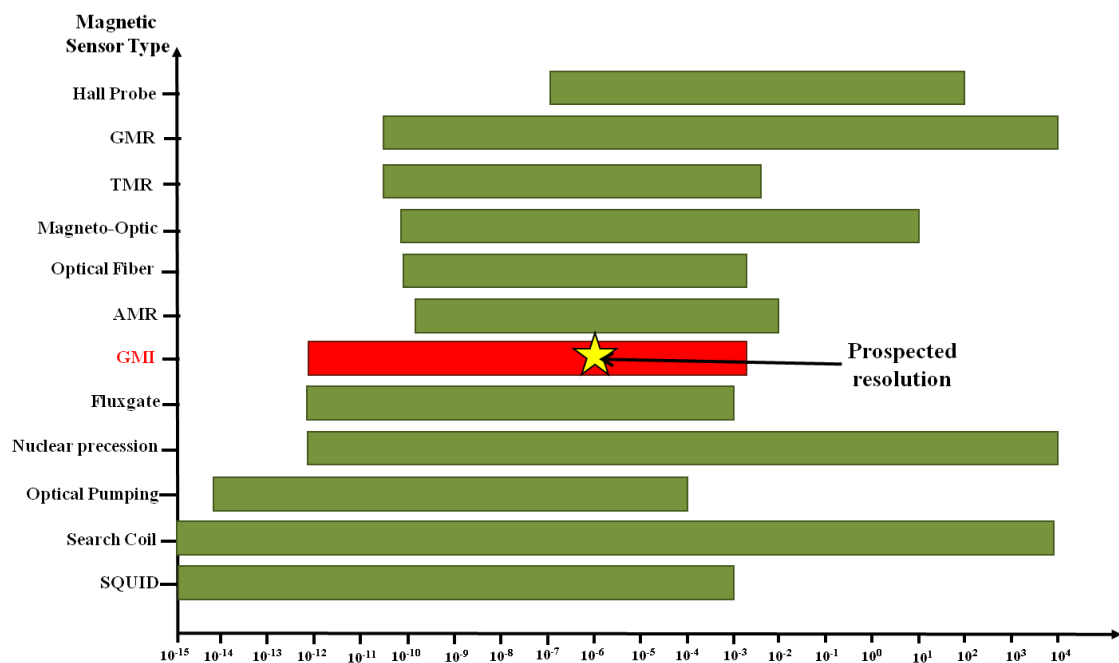


Figure 6.7 Evaluated resolution of fabricated sensor element. Star maker denotes the prospected resolution.

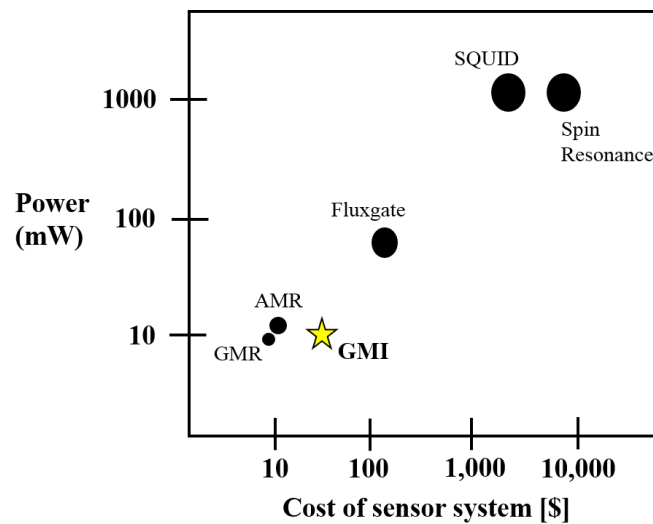


Figure 6.7 Comparison of performance cost of the magnetic sensors.

element has merit of simple design with lower power consumption and lower-production cost, as shown in fig. 6.8 [18]-[20].

6.4 Summary

In this study, I introduced the results of impedance measurement. This study attempted to confirm the proposed method and sensor element which was manufactured using the proposed method. The impedance was the minimum value when there was no external magnetic field and it increased with applying of longitudinal direction external magnetic field. The tendency of impedance variation was changed by not only geometrical properties of conductive layer but also the magnetostriction constant of magnetic material. As the result, the MI sensor element, which was fabricated using the proposed method and research, showed that it worked as a MI magnetic sensor. And the rate of impedance variation could be obtained 14% (2.5%/Oe).

References

- [1] J. W. Shin, S.H. Kim, S.Hashi, and K. Ishiyama, "Control of In-plane Uniaxial Anisotropy of Fe₇₂Si₁₄B₁₄ Magnetostrictive Thin Film Using a Thermal Expansion Coefficient," *J. Appl. Phys.*, **111**, 07E511, 2012.
- [2] K. Mohri, T. Kohzawa, K. Kawashima, H. Yoshida, and L. V. Panina, "Magneto-inductive effect (MI effect) in amorphous wires." *IEEE Trans. Magn.*, **28**, 3150-3152, 1992.
- [3] S. Tanaka, Z. Aspanut, H. Kurita, C. Toriyabe, Y. Hatuskade, and S. Katsura, "Bio-application of high-Tc SQUID magnetic sensor," *J. Mag. Mag. Mat.*, **300**, 315-319, 2006.
- [4] D. L. Graham, H. Ferreira, J. Bernardo, P. P. Freitas, and J. M. S. Cabral, "Single magnetic microsphere placement and detection on-chip using current line designs with integrated spin valve sensors: Biotechnological applications," *J. Appl. Phys.*, **91**, 7786, 2002.
- [5] K. Mohri, T. Uchiyama, and L. V. Panina, "Recent advances of micro magnetic sensors and sensing application," *Sens. Actuators A.*, **59**, 1-8, 1997.
- [6] T. Kanno, K. Mohri, T. Yagi, T. Uchiyama, and L. P. Shen, "Amorphous Wire MI Micro Sensor Using C-MOS IC Multivibrator." *IEEE Trans. Magn.*, **33**, 3358-3360, 1997.
- [7] P. Delooze, L. V. Panina, and D. J. Mapps, "AC Biased Sub-Nano-Tesla Magnetic Field Sensor for Low-Frequency Applications Utilizing Magnetoimpedance in Multilayer Films." *IEEE Trans. Magn.*, **41**, 3652-3654, 2005.

- [8] S. Yabukami, H. Mawatari, Y. Murayama, T. Ozawa, K. Ishiyama, and K. I. Arai, "High-Frequency Carrier Type Thin-Film Sensor Using Low-Noise Crystal Oscillator," *IEEE Trans. Magn.*, **40**, 2670-2672, 2004.
- [9] H. Mawatari, H. Kikuchi, S. Yabukami, M. Yamaguchi, and K. I. Arai, "High-frequency-carrier type thin film magnetic field sensor for AC detection," *J. Magn. Soc. Jpn.*, **27**, 414–418, 2003.
- [10] L. V. Panina, D. Zarechnuk, D. P. Makhnovskiy, and D. J. Mapps, "Two dimensional analysis of magnetoimpedance in magnetic/metallic multilayers," *J. Appl. Phys.*, **89**, 7221–7223, 2001.
- [11] T. Morikawa, Y. Nishibe, H. Yamadera, Y. Nonomura, M. Takeuchi, J. Sakata, and Y. Taga, "Enhancement of Giant Magneto-Impedance in Layered Film by Insulator Separation," *IEEE Trans. Magn.*, **32**, 4965-4967, 1996.
- [12] V. E. Makhotkin, B. P. Shurukhin, V. A. Lopatin, P. Yu. Marchukov, and Yu. K. Levin, "Magnetic Field Sensors Based on Amorphous Ribbon," *Sens. Actuators A.*, **27**, 759-762, 1991.
- [13] S. O. Volchkov, E. Fernández, A. García-Arribas, J. M. Barandiaran, V. N. Lepalovskij, and G. V. Kurlyandskaya, "Magnetic Properties and Giant Magnetoimpedance of FeNi-Based Nanostructured Multilayers With Variable Thickness of the Central Cu Lead," *IEEE Trans. Magn.*, **47**, 3328-3331, 2011.
- [14] J. W. Shin, S.H. Kim, S.Hashi, and K. Ishiyama, "Analysis of thin-film MI sensor using the variations in impedance and the magnetic domain structure," *J. Appl. Phys.*, **115**, 17E507, 2014.
- [15] T. Uchiyama, K. Mohri, L. V. Panina, and K. Furuno, "Magneto-Impedance in Sputtered Amorphous Films for Micro-Magnetic Sensor," *IEEE Trans. Magn.*, **31**,

3182-3184, 1995.

- [16] M. Senda and Y. Koshimoto, "High Frequency Signal Response of Impedance Matched UHF Carrier Type Head," *IEEE Trans. Magn.*, **33**, 3379-3381, 1997.
- [17] K. Hika, L. V. Panina, and K. Mohri, "Magneto-Impedance in Sandwich Film for Magnetic Sensor Heads", *IEEE Trans. Magn.*, **32**, 4594-4596, 1996.
- [18] CH. Smith and RW Schneider, "Low-field magnetic sensing with GMR sensors," *Proc. Sensors Expo and Conference*, 1999.
- [19] K. Mohri, T. Uchiyama, L.P. Shen, C.M. Cai, and L.V. Panina, "Amorphous wire and CMOS IC-based sensitive micro-magnetic sensors (MI sensor and SI sensor) for intelligent measurements and controls," *J. Mag. Mag. Mat.*, **249**, 351-356, 2002.
- [20] Marina Diaz-Michelena, "Small Magnetic Sensors for Space Applications," *Sensors*, **9(4)**, 2271-2288, 2009.

Chapter 7

Conclusion

7.1 Conclusion and Discussion

In this study, I proposed a new and simple magnetic anisotropy control method using inverse-magnetostriction due to the difference in thermal expansion coefficients between the magnetic and conductive layers because the transverse orientation magnetic anisotropy is required for development of high sensitivity MI sensors.

In chapter 3, I examined the proposed magnetic anisotropy control methodology according to changes in the material of conductive layer. When the thermal expansion coefficient of the conductive layer (molybdenum) is smaller than magnetic layer's (FeSiB), a transverse magnetic anisotropy could be induced. On the other hand, if the difference between the thermal expansion coefficients of the two layers is very small (such as when the conductive layer is made of chromium) or when the thermal expansion coefficient of the conductive layer (Titanium) is larger than magnetic layer's (such as when the conductive layer is made of titanium and the magnetic layer is made

of FeSiB) a longitudinal orientation magnetic anisotropy was induced. Consequently, using the material with the smaller thermal expansion coefficient as the conductive layer is the way to induce transverse direction magnetic anisotropy.

In chapter 4, I carried out strength control of the magnetic anisotropy field based on the results of chapter 3. According to combination of ratio between magnetic and conductive layer's length and geometry change of the sensor element, I could control the magnitude of magnetic anisotropy field. From the results, the fabrication ratio of geometrical property can be established. Besides, I also considered the magnetostriction constant by changes in the magnetic materials for reduction of anisotropy field (H_k). A higher sensitivity can be obtained by decreasing the magnetostriction constant. However, if the magnetostriction constant is nearly zero or negative, magnetic anisotropy cannot be induced in the transverse direction.

In conclusion, this work verified the proposed mechanism of inducing transverse magnetic anisotropy in magnetostrictive material using the difference between the thermal expansion coefficients of the two layers by both simulations and experiments.

I strongly anticipate that this study will be helpful in controlling the sensitivity of the MI sensor. Furthermore, it can be possible to control magnetic anisotropy locally.

7.2 Suggestions for Future Work

The magnetic anisotropy control method using inverse-magnetostriction with different thermal expansion coefficients has not yet been reported. Therefore, this study gives rise to several new avenues of research.

First, a study of the annealing temperature is necessary. In this study, I considered

only the shape of thin film and magnetic materials for induction of anisotropy field. However, the annealing temperature is also an important factor in controlling magnetic anisotropy because the generated stress which induces transverse magnetic anisotropy is strongly dependent on the temperature.

Second, more precise H_k measurement methods are required. I obtained the H_k values from VSM measuring. However, the obtained H_k values are not accurate. To improve the accuracy of the measurements of magnetic anisotropy field strength, other measuring methods are needed.

Third is the influence of the substrate on the magnetic anisotropy. Until now, I have only considered the combination of the magnetic and conductive layers. Compared to thin films, the substrate is enormously thicker. Therefore, it need to clarify the influence of the substrate must be clarified.

The most important thing is the consideration of its applications. The MI sensor was proposed about 30 years ago. Even though it has a long history of the study and has performed very well, we still do not have a commercial product. Therefore, a study of the applications is required.

List of Achievements

Journal Papers

- [1] **J.W. Shin**, Y. Miwa, S.H. Kim, S.Hashi, and K. Ishiyama, "Observation of the magnetic properties according to changes in the shape of thin-film giant magnetoimpedance sensor," *IEEE Trans. Magn.*, (in press)
- [2] **J.W. Shin**, S.H. Kim, S.Hashi, and K. Ishiyama, "Analysis of thin-film MI sensor using the variations in impedance and the magnetic domain structure," *J. Appl. Phys.*, **115**, 17E507. (2014)
- [3] **J.W. Shin**, S.H. Kim, S.Hashi, and K. Ishiyama, "The Dependence of Magnetic Anisotropy on the Ratio of Thickness," *Journal of the Korean Physical Society*, **63**, 616-680. (2013)
- [4] **J. W. Shin**, S.H. Kim, S.Hashi, and K. Ishiyama, "Control of In-plane Uniaxial Anisotropy of Fe₇₂Si₁₄B₁₄ Magnetostrictive Thin Film Using a Thermal Expansion Coefficient," *J. Appl. Phys.*, **111**, 07E511. (2012)

Other Journal Papers

- [1] Y. Miwa, **J. W. Shin**, Y. Hayashi, S. Hashi, and K. Ishiyama, "Basic study of fabricating high sensitive strain sensor using magnetostrictive thin film on Si wafer", *IEEE Trans. Magn.*, (in press)
- [2] S.H. Kim, **J.W. Shin**, S.Hashi, and K. Ishiyama, "Magnetic Bearings and Synchronous Magnetic Axial Coupling for the Enhancement of the Driving Performance of Magnetic Wireless Pumps," *IEEE Trans. Magn.*, **50**, 4003404. (2014)
- [3] S.H. Kim, J.W. Shin, S.Hashi, and K. Ishiyama, Kazushi Ishiyama¹, Masaru Ozaki, and Syuji Matsumura, "Fabrication of full magnetic impeller for improvement of the magnetic properties of Pump with Power Harvester," *J. Appl.*

Phys., **111**, 07E705. (2012)

- [4] S.H. Kim, J.W. Shin, S.Hashi, and K. Ishiyama, “Novel all-in-one magnetic pump with magnetic power harvester for medical applications,” *Smart Mater. Struct.*, **20**, 035014. (2011)

International and Domestic Conference (Oral and poster)

- [1] **J.W. Shin**, Y. Miwa, S.H. Kim, S.Hashi, and K. Ishiyama, “A study of the influence of the magnetostriction constant on magnetic anisotropy of MI sensor using magnetostrictive film,” *EMSA 2014*, Wien, Austria, Jul. 2014
- [2] **J.W. Shin**, S. H. Kim, S. Hashi, and K. Ishiyama, “Observation of the magnetic properties according to changes in the shape of thin-film MI sensor,” *Intermag2014*, Dresden, Germany, May 2014
- [3] **J.W. Shin**, S. H. Kim, S. Hashi, and K. Ishiyama, “Control of the Magnetic Anisotropy and Sensitivity in the Thin-film MI Sensor,” *7th Asian Consortium on Biomedical Engineering*, Taipei, Taiwan, Nov. 2013
- [4] **J.W. Shin**, Y. Miwa, S.H. Kim, S.Hashi, and K. Ishiyama, “Analysis of Thin-Film MI sensor using the Variations in Impedance and the Magnetic Domain Structure,” *58th MMM conference*, Denver, USA, Nov. 2013
- [5] **J.W. Shin**, S. H. Kim, S. Hashi, and K. Ishiyama, “Fabrication of thin-film MI sensor using difference of thermal expansion coefficient in trilayer,” *ISAMMA*, Taichung, Taiwan, Jul. 2013
- [6] **J.W. Shin**, S. H. Kim, S. Hashi, and K. Ishiyama, “Electrical characteristic of sandwich structured thin-film,” *Annual Meeting of IEEJ.*, Nagoya, Japan, Mar. 2013
- [7] **J.W. Shin**, S. H. Kim, S. Hashi, and K. Ishiyama, “A Basic Study of Magnetic Anisotropy Strength Control Using FeSiB Magnetostrictive Thin Film,” *ICM*, Busan, Korea, Jul. 2012
- [8] **J.W. Shin**, S. H. Kim, S. Hashi, and K. Ishiyama, “Anisotropy control of magnetic thin film,” *IWPMA (PI-SMART)*, Hirosaki, Japan, Apr. 2012

- [9] **J.W. Shin**, S. H. Kim, S. Hashi, and K. Ishiyama, "Control of In-plane Uniaxial Anisotropy of $\text{Fe}_{72}\text{Si}_{14}\text{B}_{14}$ Magnetostrictive Thin Film Using a Thermal Expansion Coefficient," *56th MMM conference*, Arizona, USA, Oct-Nov. 2011
- [10] **J.W. Shin**, S. H. Kim, S. Hashi, and K. Ishiyama, "Control of Inplane-Uniaxial Anisotropy of FeSiB Magnetostrictive Thin Film," *35th Annual Conference on Magnetism in Japan*, Niigata, Japan, Sep. 2011

Other Conference

- [1] S. H. Kim, **J.W. Shin**, S. Hashi, and K. Ishiyama, "Synchronous magnetic radial coupling for magnetic multiple-pump operation," *Intermag2014*, Dresden, Germany, May 2014
- [2] S. H. Kim, **J.W. Shin**, S. Hashi, and K. Ishiyama, "Multi-scale spiral-type magnetic machine for fluid manipulation," *Intermag2014*, Dresden, Germany, May 2014
- [3] Y. Miwa, G. Kitazawa, **J.W. Shin**, S. Hashi, and K. Ishiyama, "Study on magnetic anisotropy of magnetostrictive film by difference of thermal expansion coefficient," *37th Annual Conference on Magnetism in Japan*, Sapporo, Japan, Sep. 2013
- [4] S. Hashi, Y. Miwa, G. Kitazawa, **J.W. Shin**, S. Agatsuma, and K. Ishiyama, "Arbitrary anisotropy control of magnetostrictive film using nonmagnetic laminated layer," *SMM21*, Budapest, Hungary, Sep. 2013
- [5] S. H. Kim, **J.W. Shin**, S. Hashi, and K. Ishiyama, "Magnetically-levitated mechanism using magnet arrays for a magnetic wireless blood pump," *International Conference of ICAUMS*, Nara, Japan, Oct. 2012
- [6] S. H. Kim, **J.W. Shin**, S. Hashi, and K. Ishiyama, "A new definition of magneto-mechatronics and applications," *ICM*, Busan, Korea, Jul. 2012
- [7] S. H. Kim, **J.W. Shin**, S. Hashi, and K. Ishiyama, "Fabrication of a Fully Magnetic Impeller for Improvement of the Magnetic Properties of a Blood pump," *56th MMM conference*, Arizona, USA, Oct-Nov. 2011

Award

- [1] “For Outstanding Oral Presentation Award,” *7th Asian Consortium on Biomedical Engineering*, Nov. 2013
- [2] “Incentive Award for Poster Presentation,” *IWPMA(PI-SMART)*, Apr. 2012

Acknowledgement

I can't believe that the time has come to write the most pleasant part of my dissertation.

I would like to take this opportunity to express my gratitude to all those who supported me through the peaks and valleys of my journey through graduate school at Tohoku University. First and foremost, I would like to express my deepest thanks to Professor Kazushi Ishiyama, my research supervisor at Research Institute of Electrical Engineering (RIEC), Tohoku University, for his continual encouragement, strong support/guidance, and valuable advice throughout this process. His enthusiasm, guidance and wealth of technical knowledge provided excellent inspiration and insight for my research. I am also very grateful for his valuable suggestions and help regarding many other aspects of my life.

I would also like to acknowledge my research advisor, Associate Professor Shuichiro Hashi at RIEC, Tohoku University. He has been my mentor, my confidant, my colleague, and a never-ending source of moral support. He has been given so much of himself to help me succeed. I would also like to thank the rest of my thesis committee for their support. Prof. Muraoka and Prof. Sahashi provided me with invaluable advice and comments on both my research and my future research career plans.

I would also like to express my deep gratitude to Prof. Kwang-Ho Shin at Kyungsung University. He gave me a lot of advice on how to formalize the logical forms for one of the engineer. I cannot thank him enough for his kindness and willingness to advise me. In addition, I would like to thank Prof. Young-Hak Kim at Pukyong National University.

In particular, this work would not have been possible without the support of Ishiyama

lab members, especially Shigeto Agatsuma. Further, I thank Dr. Sung-Hoon Kim, Dr. Kyoung-Ho Kim, and Dr. Goon-Ho Park for providing me with a relaxed environment in which to live in Sendai.

I am also much indebted to Mr. Sung-Yong Shin and Dr. Sung-min Beak who are my seniors of my college days in Korea. Their hard work in Japan encouraged me to study in Japan, and it is not an exaggeration even if I say that there is not what I am without their encouragement.

I would also like to thank my best friend, Hong-Jun Choi. Even when I was in a deadlock and felt loneliness in Japan, he always walked beside me.

Finally, I would like to dedicate this work to both of my families in Korea and Japan; my father Gui-Yong Shin, my mother Hye-Kyung Kim, my sister Yul-Hee Shin, her husband Sang-Woong Park, their children, my grandmother-in-law Yoshiko Kato, my father-in-law Kenichi Kato, my mother-in-law Keiko Kato, and my wife Makiko Kato. Without their unending support and love from childhood to now, I never would have made it through this process or any of the tough times in my life. Thank you very much.